HYDROLOGICAL MODELING FOR FLOOD RISK MANAGEMENT AND MITIGATION EFFORTS IN THE RHINE RIVER BASIN

Thesis by
Julia Grace Litong Kraatz

Supervised by
Prof. Dr. Edzer Pebesma (WWU)

Co-Supervised by
Moritz Hildemann (WWU)
Dr. Sergio Trilles (UJI)

In Partial Fulfillment of the Requirements for the
Degree of
Master of Science in Geospatial Technologies

Westfälische Wilhelms-Universität Münster (WWU),
Universidade Nova de Lisboa (UNL), Universitat Jaume I
(UJI)

Münster, Germany

2023
Defended on January 27, 2023

ACKNOWLEDGEMENTS

I would like to acknowledge and give many thanks to my supervisors, Prof. Dr. Edzer Pebesma, Moritz Hildemann, and Dr. Sergio Trilles. Thank you for your questions, your input, and your guidance which helped to shape this work. I was very fortunate to have such knowledgeable and dedicated people from the Geospatial world provide me with support during this thesis process.

I would also like to thank the amazing people from the Joint Research Center (JRC), Stefania Grimaldi, Jesús Casado Rodriguez, and Carlo Russo. This work would not have been possible without you. Thank you for answering email chains that go far beyond what Gmail is used to, and for helping me understand not just the technical aspects of the model, but also in my understanding of hydrological processes. Your kindness will not be forgotten, and I wish you all the best.

Finally, I would like to thank my family and friends for all their love and support.

To my family: thank you for always believing in me, even when I didn't believe in myself. As Alec Baldwin writes, "The longer I live, the more deeply I feel that love…is the work of mirroring and magnifying each other's light…in those moments when life and shame and sorrow occlude our own light from our view, but there is still a clear-eyed loving person to beam it back. In our best moments, we are that person for one another." Thank you for beaming it back, time and time again. Not just in this thesis, but in my life. Love and aloha, always.

To my friends: thank you for endless laughs, talks, and for bringing joy into my life. I guess you must think I'm kind of cool since you've stuck around for this long—I hope you know I think you're all amazing, and that I'm so grateful we could share some of this life together. Wherever the world takes you, I wish you happiness.

ABSTRACT

Urban flooding is a global issue that affects millions of people every year. It is the most frequent natural hazard to affect large cities, and causes numerous damages to personal property, city infrastructure, and in some cases loss of life. In July of 2021, western Germany was greatly impacted by urban flooding; from the 14 to 15th of July, more than 180 lives were lost due to intense rainfall and flooding, with more than 40,000 people affected. In this work the flooding of 2021 was modeled within the Upper Rhine River basin using the LISFLOOD-OS hydrological model, to conduct a flood-risk analysis in one of the most impacted states during the flooding even, Rhineland Pfalz. Further, the calibrated model was run with higher levels of precipitation to determine possible risks associated with a future flooding event in the same region. To calculate flood-risk, flood depth-damage functions were implemented on simulation outputs to determine flood-risk. Reliability of the flood-risk analysis was done by comparing Copernicus monitored flood extent data from the flooding event against the flood-risk classification map. Results show that the flooding event of 2021 could be modeled with reasonable discharge levels compared to observations from the Mainz gauging station, producing a KGE score of 0.438; further, land use classes which received the highest damage values in both the simulated flooding event of 2021 and in the future flooding event scenario were agricultural and residential areas. High-risk areas from the flood simulation of 2021 fell within Copernicus monitored flood extent areas, highlighting the potential of this methodology to be applied to future flood-risk management practices.

Keywords: LISFLOOD, flooding, hydrological modeling, flood-risk, Germany

TABLE OF CONTENTS

LIST OF FIGURES

LIST OF TABLES

Chapter 1

INTRODUCTION

Urban flooding is a dangerous and costly natural hazard which occurs on a global scale, and causes numerous damages to personal property, city infrastructure, and in some cases loss of life (Bosseler et al., 2021; Surminski & Thieken, 2017). It is an issue that affects millions of people every year, and annually contributes to 40 percent of the world's total economic losses from natural hazards (Afsari et al., 2022). Over the past few decades, the impacts of flooding have been increasing due to climate change and socioeconomic developments (Surminski &Thieken, 2017); as reported by the IPCC, the frequency and intensity of heavy precipitation events has increased in North America and Europe, which is linked to human impacts that has caused changes in weather and climate patterns (IPCC 2014). Furthermore, since surface temperature is projected to rise throughout the 21st century, it is extreme precipitation events will likely continue to increase in intensity and frequency in many regions, albeit not equally throughout the globe (IPCC 2014).

In addition to climate change, socioeconomic developments, such as population increase, centralization, and industrialization and urban growth, have also contributed to the increase in extreme precipitation events (Surminski & Thieken, 2017). Urban growth is particularly problematic with regard to flooding because it leads to an increase in impervious surfaces and a reduction of pervious surfaces. This in turn prevents groundwater recharge and disrupts evapotranspiration losses, subsequently causing an increase in surface runoff, which puts urban settlements at greater risk of major flooding events (Ajjur & Al-Ghamdi, 2022). Thus, climate change, along with changes humans have imposed on the environment, has caused extreme flooding events to occur more frequently on a global scale (Gai et al., 2019). As more than two thirds of the world's population is expected to reside in urban settings by the year 2050, this means that as time goes on a greater proportion of the world's population will be at a higher-risk of living in a flood-prone area, and therefore vulnerable to the negative repercussions of flooding and major flooding events (Tom et al., 2022).

Effective flood mitigation efforts are thus imperative for the future of urban settlements. Governments around the world are increasingly partaking in flood risk management (FRM) practices, which attempt to address flood risks in an anticipatory way, rather than after the disaster occurs (Surminski & Thieken, 2017). FRM practices usually include measures such as planned and controlled land-use within cities, soil conservation efforts, agroforestry practices, drainage maintenance, and sustainable practices for city planning and development (Tom et al., 2022). Flood insurance also has the potential to spur FRM efforts, such as encouraging flood proofing of buildings and properties, retrofitting houses, local

flood protection measurements, and the building of large-scale protection schemes (Surminski & Thieken, 2017).

Specifically in Germany, the flood hazard zoning system (ZÜRS) was established in 2001 by the German Insurance Association (GDV) (Surminski & Thieken, 2017) in order to categorize areas with different flood probabilities (Seifert et al., 2013). The zoning system initially contained three flood probability zones, but after the Elbe and Danube River flooding in 2002, a fourth zone was added for areas with low flood probabilities (Surminski & Thieken, 2017). Most properties in Germany are in exposure zone 1, which is defined as a flood probability lower than 1/200 years. Properties in zone 1 are considered insurable. Another 10 to 12 percent of properties in Germany are in exposure zone 2, with flood probabilities between 1/50 and 1/200 years, and approximately 3 percent of properties are in exposure zones 3 and 4, with a flood probability of between 1/10 and 1/50 years, meaning that these zones have a high likelihood of being flooded (Seifert et al., 2013).

ZÜRS was based on a coarse DEM and a rough hydraulic modeling approach, which was initially heavily criticized by water authorities in Germany. New maps were therefore implemented into the system, and since 2014 these more sophisticated maps were incorporated into ZÜRS (Seifert et al., 2013). However, even with these changes to the zoning system, it is still difficult for homeowners to obtain flood insurance (Surminski &Thieken, 2017). This could be due in part to the fact that state governments have authority over flood defense and administration (Seifert et al., 2013); while the federal government of Germany may set general standards, it is ultimately up to the federal states (Länder) to determine the framework legislation and implement actual management strategies within the state (Surminski &Thieken, 2017).

Another reason it is difficult for homeowners to obtain flood insurance, even in zones that have already been affected by 10-year floods, is because insurers can suffer many losses during a single flood event (Seifert et al., 2013). Insurance companies in Germany are not required to share flood risk information with their customers, which means that many people may be unaware of the risks they face, and therefore do not buy flood insurance (Surminski & Thieken, 2017).

Thus, while FRM practices are in progress in places like Germany, by means of insurance and other governmental initiatives, FRM practices worldwide are still not as advanced as they need to be to aid urban populations in times of major flooding events. In truth, most FRM measures often take years to implement, and are dependent on national or local governments to enact. As of 2017, globally only 12 percent of funds for disaster management were invested in risk reduction measures, while 88 percent were used in response, either during or after the disaster event (Surminski & Thieken, 2017). As a result of this, one of the main mechanisms for flood prediction and response is through early warning systems.

1.1 EFAS and the LISFLOOD Model

Since major flooding events can occur quite rapidly, understanding the hydrological processes behind potential flooding events is important for management and mitigation efforts; this is done through early warning systems, which often-times take advantage of hydrological models, the focus of this work. As climate change is projected to increase risks for people, assets, economies, and ecosystems, including but not limited to risks from extreme precipitation (IPCC 2014), having flood forecasting and early warning systems aids governments and institutions responsible for evacuating people, and can help to prevent damages to assets in a timely manner (Cantoni et al., 2022). In Europe, flood forecasting and early warning systems are managed at both national and regional levels, and are complemented at a European scale by the European Flood Awareness System (EFAS), which was implemented in 2005 (Cantoni et al., 2022).

EFAS was developed by the European Commission to provide operational flood predictions in major European rivers as part of the Copernicus Emergency Management Services (Dottori et al., 2017). EFAS is responsible for flood warning (Dottori et al., 2017), with the aim of providing national hydrological services with continuous real-time river discharge forecasts across Europe at a lead-time of 3-10 days (Feyen et al., 2007). The hydrological simulations within EFAS are performed based on the LISFLOOD-OS hydrological model (Dottori et al., 2017), the model which will be implemented in this work.

1.2 Motivation

In the past decades, some of the costliest floods have occurred in central Europe (Shustikova et al., 2019). The flooding which occurred in western Germany and bordering countries during the summer of 2021 was no exception; for Germany alone, this flooding event cost upwards of 40 billion euros in damages (Reuters, 2022). The flooding began with rain in the early morning of the 14th of July with records from the Cologne-Stammheim DWD weather station at 04:00 UTC (Mohr et al., 2022). The rain then reached the Ahr catchment, and by 09:30 UTC the entire catchment was covered. Around noon the precipitation intensified, and the highest precipitation levels were recorded. Within 15 hours on the 14th of July, 2021, 150 mm of precipitation fell. This equated to more than twice the usual monthly precipitation in just a few hours (Mohr et al., 2022), and was classified as a pluvial flood, a flood which occurs in cities and is caused by intense rainfall (Tom et al., 2022).

From the 14th to 15th of July, 2021, more than 180 lives were lost due to intense rainfall and flooding, with estimates of up to 40,000 people affected. The two Bundesländer (Federal States) which were impacted the most by this flooding event were North-Rhine Westphalia and Rhineland Pfalz (Fekete & Sandholz, 2021). For civilians and researchers alike, this turn of events came unexpectedly. Not only did the flooding cause extreme damage both socially and economically (Fekete &

Sandholz, 2021), but it also exposed major flaws in the flood management system in Germany (Bosseler et al., 2021).

In the aftermath of the 2021 floods in Germany, Fekete and Sandholz (2021) conducted a survey on 2,264 participants, which included respondents from the local and Federal administration, crisis managers, flood experts, and civilians (Fekete & Sandholz, 2021). Their survey revealed that missing information was reported as a constraint in flood-management operations for 51 percent of respondents (Fekete & Sandholz, 2021). Although the European flood directive funded research for flood hazard and risk maps considering the flood events of 2002 at the Elbe and Danube rivers, in the east and south of Germany respectively, this work was discontinued in 2012 due to conflicts between the 16 Bundesländer states (Fekete & Sandholz, 2021). Thus, in the current day-and-age, many German cities do not have high-resolution riverine, groundwater, and pluvial flood maps, making it difficult to identify vulnerable populations (Fekete & Sandholz, 2021). Although the European flood directive is responsible for addressing all different types of floods, such as riverine, pluvial, and storm surges, pluvial floods are largely neglected in Germany. Instead, the focus has been on riverine floods and storm surges that could affect the country on a national level, contributing to a lack of preparation for pluvial flooding events, such as the flooding which occurred in 2021 (Surminski & Thieken, 2017).

Thus, the motivation for the study area of this work is the Rhineland Pfalz region, which was greatly impacted by the flooding event of 2021. Additionally, a hydrological model was implemented in this work because hydrological models not only simulate processes which occur within a catchment, but also allow for geospatial analysis of where hydrological processes, such as water discharge, occur. This is an advantage over purely probabilistic approaches and was the motivation for using a hydrological model. Further, since climate change and urbanization have increased the occurrence and frequency of flooding events, this work is motivated to produce a future flooding event scenario within the study area, to exemplify one approach of a FRM practice that could aid governments and civilians in future flood mitigation efforts.

1.3 Research Questions and Objectives

The objective of this research is to use the LISFLOOD-OS hydrological model in the Upper-Rhine River Basin to simulate the flooding which occurred in July of 2021, and conduct a flood-risk methodology. Further, this work will apply the risk analysis in a future flooding event scenario, in order to project future impacts. The main questions which will guide this research are:

1) How closely can flooding levels from 2021 be modeled with the LISFLOOD model, and produce a future flooding scenario?

2) Which land use classes within the Rhineland Pfalz region received the highest damage values in the flooding event of 2021, according to the EU flood depth-damage values? How do these values change in a future flooding scenario?

Chapter 2

LITERATURE REVIEW

2.1 Hydrological Models and Approaches to Flood Modeling

In the body of flood modeling literature, there are a wide range of hydrological models that are used for flood simulation. In general, hydrological models have vastly improved in the last few decades due to increased computational power and progress in data acquisition (Hdeib et al., 2021). Within hydrological models, there are a few different types: namely, conceptual, physically based, and event based. Conceptual models have parameters which are calibrated against observed discharge and are mostly used for flood forecasting (Peredo et al., 2022). Physically based models, such as LISFLOOD, can run without calibration; however, they require a large amount of field data and require high computational time (Peredo et al., 2022). Event based models have a fast computational time in comparison to continuous models, however they require a high amount of effort regarding estimating the catchment's initial conditions (Peredo et al., 2022). Regardless of the modeling approach, however, all hydrological models aim to reproduce a catchment's dynamics in response to a rainfall event (Peredo et al., 2022), which can then aid in planning efforts to minimize flood damages.

Hdeib et al. (2021) produced a cost-performance analysis grid comparing different flood modeling approaches (Hdeib et al., 2021). They defined the relative 'cost' of a model based on the model type and model code (Hdeib et al., 2021). In terms of hydrological model type, this included seven evaluation criteria which included spatial scale, temporal scale, number of events (if event-based) or duration (if continuous), nature of the basic algorithm, spatial representation, computational time step, and flow processes represented (Hdeib et al., 2021). For model code cost, they defined the building of new code as more costly, because of the time and expertise employed; additionally, if new modeling software had to be purchased, this was considered more costly than open source (Hdeib et al., 2021). Results from the cost-performance grid showed that a coupling model done by Montanari et al. (2009) in Luxembourg on the Alzette River had the highest performance. The model with the lowest cost was conducted by Samela et al. (2018) in Romania on the Danube River and was an empirical and geomorphic model (Hdeib et al., 2021).

Peredo et al. (2022) investigated the potential of the conceptual, hourly, semi-distributed hydrological model, GRSD model, in the Mediterranean region in southwest France (Peredo et al., 2022). The authors of this study modified the model by explicitly accounting for rainfall intensity, to improve the simulation of extreme flood events in this region, which is particularly prone to flash floods (Peredo et al., 2022). The GRSD model runs at hourly time steps and propagates river flows downstream between lumped modeling units from sub-catchments to the main outlet (Peredo et al., 2022). The modified model structure was performed

over a 10-year period of hourly flow observations, along with 31 gauged sub-catchment simulations for 4 flood events (Peredo et al., 2022). Through Kling Gupta Efficiency (KGE) criterion of model performance, it was found that the model adaptation did not deteriorate model simulations when compared to the original GRSD simulations (Peredo et al., 2022). Additionally, the adapted GRSD model performed better for the four flood events, meaning that for future flood events in this region, the modified GRSD model could better forecast possible damages and human losses (Peredo et al. 2022). The model modification also demonstrates the model's versatility, in that the addition of accounting for rainfall could be calibrated successfully with accurate results (Peredo et al., 2022).

Ruijsch et al. (2021) utilized the PCR-GLOBWB model to investigate systemic change in the Rhine-Meuse basin. The PCR-GLOBWB 2.0 model is a global hydrological model which consists of 5 modules: the meteorological forcing module, the land surface module, the groundwater module, and the surface water routing module (Ruijsch et al., 2021). These modules calculate within a daily time step the water storage in two soil layers and the underlying groundwater layer. They also calculate the exchange between these layers, snow storage, interception storage, and atmosphere (Ruijsch et al., 2021). The authors of this study calibrated the model using brute-force calibration, which means that all possible parameter combinations were run for each given step size during the period of 1901-2010 (Ruijsch et al., 2021). Similar to other works (Cantoni et al., 2022; Gai et al., 2019; Hirpa et al., 2018; Peredo et al., 2022), the objective function which was used to find the best-fitting parameter values was KGE, which measures correlation, variability, and bias to determine the model's overall skill (Ruijsch et al., 2021). To model systemic change, the authors of this study compared three different calibration scenarios, and found that systemic change did occur in the Rhine-Meuse basin, possibly due to climate change, land use change, and river structure (Ruijsch et al., 2021).

Ryan et al. (2022) used the TUFLOW 2-dimensional hydraulic model in three different use-cases, comparing flood flows with the varying effects of Manning's *n* values, cell size, infiltration, and subsurface flows. Unlike Peredo et al. (2022) and Ruijsch et al. (2021), this study conducted a manual calibration of the model parameters to simulate flood flows. They found that sub-grid sampling (SGS), a technique which resamples the Digital Elevation Model (DEM) to ensure that low flows are represented in flow paths narrower than the grid cell, significantly improved flood simulations (Ryan et al., 2022).

Similar to Shustikova et al. (2019), Quirogaa et al. (2016) demonstrated the effects of varying Manning's *n* values using the HEC-RAS model in three separate catchments. They found that calibration through Manning's *n* values could be achieved to produce normal values compared to observations, by including a subsurface flow mechanism. They also found that direct rainfall model simulations improved with Sub-Grid Sampling (SGS), a technique with resamples DEMs to a higher spatial resolution to ensure that low flows are represented for flowpaths narrower than the 2D cell size (Quirogaa et al., 2016).

2.2 The LISFLOOD Hydrological Model

The model which will be implemented in this work to simulate the flooding event of 2021 and a future flooding scenario is the LISFLOOD-OS model. It should be noted that the term LISFLOOD will be used in this work referring to the LISFLOOD-OS model, with LISFLOOD-FP referring to its sister model. The LISFLOOD model is a 2-dimensional GIS-based hydrological rainfall-runoff model, capable of simulating hydrological processes that occur in a catchment (Van Der Knijff et al., 2010). The model is raster based, which means that simulated hydrological processes are applied to each cell within a 2D grid (Feyen et al., 2007; Ryan et al., 2022). The LISFLOOD model was developed specifically for hydrological processes which occur in large European river basins, and can be used in a variety of different use-cases, such as flood forecasting, assessment of the effects of river regulation measures, land-use changes, and climate change (Van Der Knijff et al., 2010). The LISFLOOD model is written in a combination of PCRaster Dynamic Modelling Language and Python scripting language, and is a widely used model within the body of hydrological modeling literature. For example, Cantoni et al. (2022) used the LISFLOOD model for flood modeling in Tunisia. They used the Distributed Evolutionary Algorithm for Python (DEAP) for model calibration, and found that simulations without model calibration were strongly biased. The conclusions of this work surmised that there is a need for the development of river discharge databases to help with flood warning systems, such as EFAS or the Global Flood Awareness System (GloFAS) (Cantoni et al., 2022).

Hirpa et al. (2018) also used the LISFLOOD model in their analysis for the calibration of GloFAS, which utilizes the LISFLOOD model. In GloFAS, the model is run at a daily time step with a 0.1° resolution (Hirpa et al., 2018). Similar to Cantoni et al. (2022), the authors of this study also used the DEAP for model calibration, and found that the calibration of the model parameters improved the overall simulation of streamflow: however, also noted that these results could vary across regions (Hirpa et al., 2018).

Feyen et al. (2007) implemented the LISFLOOD model on a daily time-step for the Meuse catchment. They used the Shuffled Complex Evolution Metropolis (SCEM-UA) global optimization algorithm for the automatic calibration of daily discharge observations to simulate streamflow. The authors of this study found that the SCEM-UA algorithm was able to converge to target posterior parameter distributions in less than 2500 iterations. This exemplified the versatility of the model with the use of different calibration algorithms, and applicability of LISFLOOD to European catchments (Feyen et al., 2007).

Knighton et al. (2020) used the LISFLOOD-FP model in their work on predicting flood insurance claims with machine learning. Using the physically-based LISFLOOD-FP model, they found that estimating flood hazard areas overlapped with 57 and 45 percent of historical insurance claims. They also found through a random forest classification that the flood generated claims were captured within the Hackensack and Moodna catchments, at 80.6 and 93.2 percent respectively.

This study demonstrated the ability of the LISFLOOD-FP model to be incorporated with socio-economic data in order to produce estimates of flood-risk (Knighton et al., 2020).

Gai et al. (2019) used the LISFLOOD model to test flood management practices in the Wei River Basin, China. They analyzed flooding events and low flow characteristics with different human intervention scenarios, and found that the construction of reservoirs in the Wei River Basin may reduce the occurrence of floods; further, they found that water diversion plans have the possibility of increasing low flow while not increasing flood risk (Gai et al., 2019). Like Cantoni et al. (2022) and Hirpa et al. (2018), the authors of this study also used the DEAP for model calibration, along with KGE, Nash-Sutcliffe model Efficiency (NSE), and Percent Bias (PBIAS) as the objective functions. While this application of LISFLOOD was not in a European catchment, it demonstrates how the LISFLOOD model can be applied outside of Europe as well.

Shustikova et al. (2019) compared the LISFLOOD-FP model with the HEC-RAS model to demonstrate each models' ability to simulate inundation over complex topography over an initially dry floodplain. They used 2D formulations for both models in order to focus on floodplain wave dynamics present in each model. They used Manning's roughness coefficients for model calibration and found that the overall performance of the LISFLOOD-FP in simulating inundation extent was slightly better than HEC-RAS. At 25m spatial resolution, the LISFLOOD-FP was able to capture 81 percent of flood extent within the study area, whereas the HEC-RAS model at the same resolution captured 78 percent of the flood extent. The authors of this study concluded that overall, the LISFLOOD-FP model was able to capture flood extent and water depth at water marks (measured from the flood event) better than the HEC-RAS model, however that the HEC-RAS model was able to capture the spatial distribution (i.e., the inundation boundary) of the flood event better than the LISFLOOD-FP model. Thus, the authors conclude that model selection is dependent on the study aim (Shustikova et al., 2019).

2.3 Risk Assessment and Approaches to Quantifying Flood Risk

Within the body of literature which use hydrological models for the quantification of flood-risk, approaches and methodologies were found to be scarce or lacking. While early warning systems are used to predict flood magnitude, there is a gap with regard to their ability to translate flood forecasts into flood risk evaluations (Dottori et al., 2017). From all the literature that was analyzed in this work, only one was found to use the LISFLOOD model with a flood-risk analysis. Thus, in this section the methodologies for quantifying flood risk which were found within the literature review will be discussed, finally detailing the one which will be implemented in this work using the LISFLOOD model.

Ajjur and Al-Ghamdi (2022) used the physically-based hydrological model WetSpass to investigate water balance components and quantify surface runoff in their case study area Doha, Qatar, between the years of 1984-2020. They used five

monthly climatic parameters from six meteorological stations, the parameters being minimum air temperature, maximum air temperature, average air temperature, wind speed, and precipitation (Ajjur & Al-Ghamdi, 2022). They used air temperatures to compute potential evapotranspiration, land maps in the years of the study area, and then implemented the WetSpass model to calculate surface runoff at the country scale. The authors detailed that within the WetSpass model, precipitation measurements are separated by runoff, groundwater recharge, and actual evapotranspiration. The model also includes physical catchment properties, such as slope, soil type, and land use, along with groundwater properties such as groundwater level depth. In order to compute the nexus between urban growth, climate change, and flood risk, the authors of this study used a Pearson Correlation to verify the connection between these three variables, where urban growth was calculated as the percentage of urban growth which changed during the duration of the study, flood risk was represented by the simulated surface runoff by the WetSpass model, and climatic factors were calculated by using the hydrological model.

El-Saoud & Othman (2022) used the 2D hydraulic model HEC-RAS in combination with satellite data, a watershed modeling system (WMS), and the hydrological model HEC-1 to predict and simulate surface runoff in the Wadi Mehassar basin. The aim of the study was to produce spatially distributed information, such as water surface elevations, velocity, and depths, for flash-flood hazard assessment. The authors of this study first conducted a statistical analysis of the maximum and minimum daily rainfall values affecting the basin, to estimate the probability of the maximum rainfall intensities for a given period. They then delineated the boundaries of the drainage basins using the WMS program and the HEC-1 model to transform rainfall data into flow to estimate inflow volumes and peak discharge values. Next, the authors of this study used the HEC-RAS model to simulate drainage into the watershed area, which was dependent on the inflow rates produced by the HEC-1 model. Finally they used a geomatic remote sensing technique for data processing of the simulation output in order to delineate the flash flood zones and exposed areas (El-Saoud & Othman, 2022).

Afsari et al. (2022) used the fuzzy analytic hierarchy process (FAHP) to determine weights and ordered weighted average (OWA), to create a vulnerability map for flooding in Tehran under different risk scenarios. They implemented this methodology by first identifying important criteria for determining vulnerability in urban areas with regards to floods; they did this through literature search, and then presenting a questionnaire on criteria weighting to experts. Next, this information was input into GIS maps, with the assigned weighted criteria. The authors then applied the weighting method, FAHP, followed by the application of minimum and maximum functions for dimensionless criterion mapping. The criteria map was then combined with the OWA model, which delineated areas which would be vulnerable to flooding and respective degrees of risk. Finally, the model results were evaluated using a sensitivity analysis (Afsari et al., 2022).

Wang et al. (2019) used general circulation models (GCM) in combination with a hydrological model to assess the overland flood risk affected by climate change and hydraulic engineering in Baiyangdian Lake Area (BYD), located south of Beijing, China. They used five GCM models, HadGEM2-ES, GFDL-ESM2M, ISPLCM5A-LR, MIROC-ESM-CHEM, and NorESM1-M, and one hydrological model, the variable infiltration capacity (VIC) model. They used the VIC model to simulate infiltration and excess runoff generation, and the hydrodynamic GCM models to implement three flooding scenarios; one scenario with a historic 50 year flood, a second with a historic 50 year flood along with a heightened dike of 2 m and reservoirs, and finally a future scenario with a heightened dike of 2 m and reservoirs. The results of this study found that flood risk was relatively high in the local district of the BYD under the future climate change scenario (Wang et al., 2019).

The flood risk methodology in this work was inspired by the methods implemented by Dottori et al. (2017), who used the LISFLOOD model to implement a rapid risk assessment procedure for Europe. They did this by first simulating streamflow and flood forecasting, secondly conducting event-based rapid flood hazard mapping, and finally producing an impact assessment. The authors of this study calibrated the LISFLOOD model at a European scale using streamflow data from several gauging stations, and interpolated meteorological data based on point measurements of precipitation and temperature. They ran the model on a 5km grid and used an initialization period of 1990-2013 for proceeding LISFLOOD runs. Then, using available flood forecast data which is provided by EFAS with a lead time of 10 days, river sections potentially affected by local flood magnitude were identified through the return period of peak discharge. Next, areas at risk of flooding were determined by use of a map catalog, with flood-prone areas delineated based on flood magnitude. These flood maps were then compared to local flood protection measures and merged into an event-based hazard map. The authors of this study then combined these event hazard maps with exposure and vulnerability information to assess affected population, infrastructure, urban areas, and economic damage, based on the normalized damage functions developed by Huizinga et al. (2007) (Dottori et al., 2017).

Chapter 3

METHODOLOGY

The following chapter describes the methodology carried out in this work. Figure 1 shows the general outline of the steps taken to produce the results, with each subsection of this chapter detailing the specifics on the procedures which were implemented.
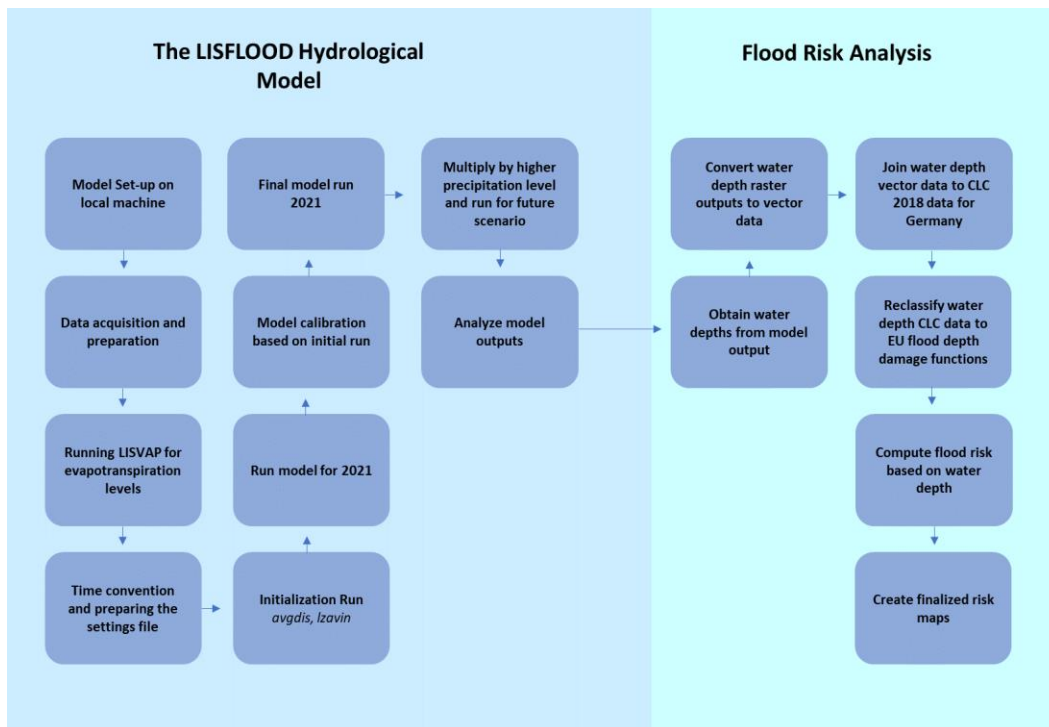

Fig. 1 Methodology flow chart for the steps and processes carried out in this work.

3.1 Study Area

The Rhine River is one of the largest rivers in Europe. It has origins in the Swiss Alps and flows through several countries, including Germany, Switzerland, and the Netherlands, eventually ending in the North Sea (Ruijsch et al., 2021). The Upper Rhine River Basin, the study area of this work, is a hydrological entity which spans across Germany, Luxembourg, Belgium, and Switzerland. It has an area of approximately 140,929km^2, and includes the German State Rhineland Pfalz, which was flooded in July 2021. It should be noted that hydrological processes which are simulated within the LISFLOOD model must occur within a catchment. Thus, the Upper Rhine River Basin was chosen as the study area of this work because it included the Rhineland Pfalz region.
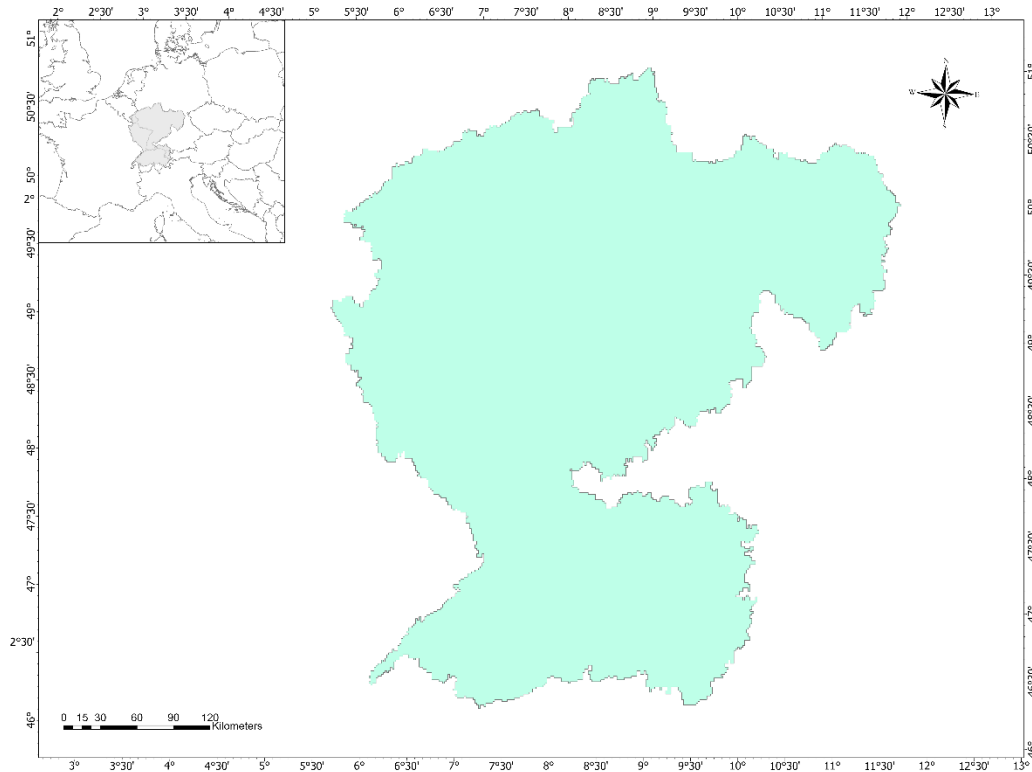
Fig 2. Study area, the Upper Rhine River Basin (author)

3.2 The LISFLOOD Model

3.2.1 Simulated Hydrological Processes

The LISFLOOD model is able to simulate a multitude of hydrological processes, including snow melt, infiltration, interception of rainfall, leaf drainage, evaporation and water uptake by vegetation, surface runoff, preferential flow, soil moisture distribution, drainage to the groundwater, sub-surface as well as groundwater flow, reservoirs and river channel routing (Gai et al., 2019).

In this work, all hydrological processes related to surface-runoff were simulated within the model to produce flood discharge levels. These hydrological processes will be explained in the following section. Excluded hydrological processes which were not modeled include snowmelt and lakes, since there were no large lakes present in the study area and the study area was not affected by snowmelt. A conceptual model which documents an overview of hydrological processes simulated within the model can be found in Figure 3. Further documentation on snowmelt and lake processes which can be simulated within the LISFLOOD model can be found in Van Der Knijff et al. (2010).
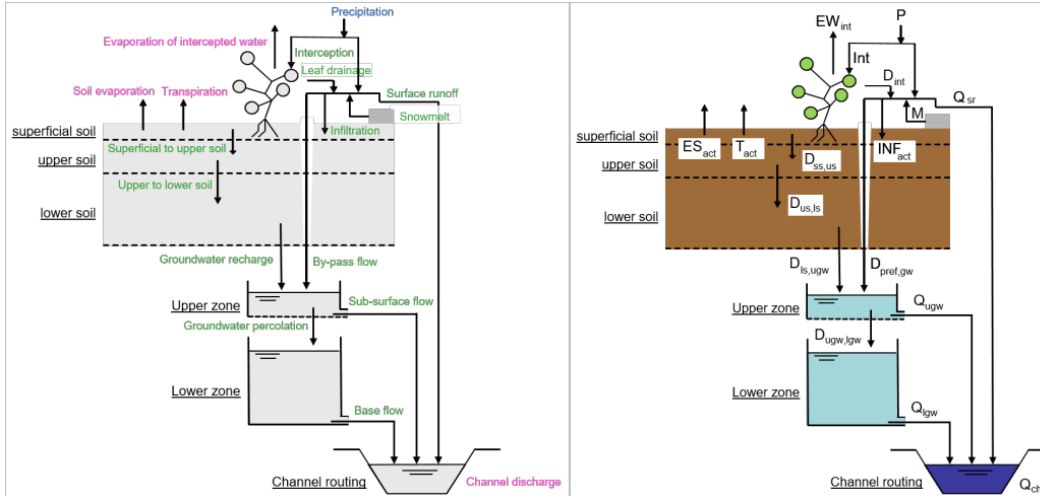
Fig 3. Conceptual model of the LISFLOOD-OS hydrological rainfall-runoff model, including hydrological processes and model variables. *P*=precipitation; *Int*=interception; *EW$_{int}$*=evaporation of intercepted water; *D$_{int}$*=leaf drainage; *D$_{int}$*=leaf drainage; *ES$_a$*=evaporation from soil surface; *T$_a$*=transpiration (water uptake by plant roots); *INF$_{act}$*=infiltration; *R$_s$*=surface runoff; *D$_{1,2}$*=drainage from top-to subsoil; *D$_{2,gw}$*=drainage from subsoil to upper groundwater zone; *D$_{pref,gw}$*=preferential flow to upper groundwater zone; *D$_{uz,lz}$*=drainage from upper to lower groundwater zone; *Q$_{uz}$*=outflow from upper groundwater zone; *Q$_l$*=outflow from lower groundwater zone; *D$_{loss}$*=loss from lower groundwater zone. Snowmelt is not included in this figure although it is able to be simulated within the LISFLOOD-OS model (*LISFLOOD Model Documentation*, n.d.; Van Der Knijff et al. 2010).

Rainfall interception is modeled within the LISFLOOD-OS model using the approach of Aston (1979) and Merriam (1960) using two parameters. Where interception is estimated as:

$$Int = S_{\max} \cdot [1 - \exp(-k \cdot R \Delta t / S_{\max})] \tag{1}$$

where *Int* (mm) is the interception per time step, *S$_{max}$* (mm) is the maximum interception, *R* is the rainfall intensity (mm day $^{-1}$) and *k* accounts for vegetation density (Van Der Knijff et al., 2010). *S$_{max}$* is calculated using the empirical equation (*LISFLOOD Model Documentation*, n.d.):

$$\begin{cases} S_{\max} = 0.935 + 0.498 LAI - 0.00575 LAI^2 & (LAI > 0.1) \\ S_{\max} = 0 & (LAI \leq 0.1) \end{cases} \tag{2}$$

with *LAI* being the average Leaf Area Index (m^2 m^{-2}) in each grid cell, and *LAI* related to the constant *k* in the equation:

$$k = 0.046 LAI \tag{3}$$

In terms of evaporation of intercepted water, EW_{int} is the potential evaporation rate from an open water surface, *EW0,* which is defined as:

$$EW_{max} = EW0 \cdot \left[1 - \exp(-\kappa_{gb} \cdot LAI)\right] \Delta t \tag{4}$$

where EW_{max} is the maximum evaporation per time step, proportional to the fraction of vegetated area in each pixel, and k_{gb} is the constant for global solar radiation (Van Der Knijff et al., 2010). Further, evaporation from interception is defined as:

$$EW_{int} = \min(EW_{max} \Delta t, \, Int_{cum}) \tag{5}$$

with EW_{int} being actual evaporation, which occurs from interception store per time step. The LISFLOOD model assumes that all water on average either evaporates or falls to the soil surface as leaf drainage within one day, in $Int_{cum.}$ leaf drainage is further defined in the equation:

$$D_{int} = \frac{1}{T_{int}} \cdot Int_{cum} \Delta t \tag{6}$$

where D_{int} is the leaf drainage per time step in mm, and T_{int} is the time constant for interception store of one day (*LISFLOOD Model Documentation*, n.d.; Van Der Knijff et al., 2010).

In terms of impervious surfaces, the LISFLOOD model assumes that any water that reaches an impervious surface is added directly to the surface runoff, that there is no storage capacity, and that there is no groundwater storage. Direct runoff is therefore defined as (*LISFLOOD Model Documentation*, n.d.; Van Der Knijff et al., 2010):

$$R_d = f_{dr} (R * \Delta t + M - IntercSealed) + WaterFraction * (R * \Delta t + M - EW0) \tag{7}$$

For pervious surfaces, the fraction of each cell that is pervious is defined by the equation:

(8)

$$W_{av} = R\Delta t + M + D_{int} - Int$$

with *R* being rainfall intensity per time step and *Int* being rainfall interception (Van Der Knijff et al., 2010).

For evapotranspiration, simulated processes are modeled after the widely-used FAO Penman-Monteith method, where vegetation transpiration and water uptake are modeled separately from direct evaporation from the soil surface. This enables historical data to be used as input into the LISFLOOD model (Van Der Knijff et al., 2010). Maximum transpiration per time step is defined as:

$$T_{max} = k_{crop} \cdot ET0 \cdot \left[1 - \exp\left(-\kappa_{gb} \cdot LAI\right)\right]\Delta t - EW_{int}$$ (9)

with *ET0* being the potential (reference) evapotranspiration rate per day, and k_{crop} being the crop coefficient. In case of water stress, the LISFLOOD model reduces the transpiration rate with a reduction factor, defined as:

(10)
$$r_{ws} = \frac{w_1 - w_{wp1}}{w_{crit1} - w_{wp1}}$$

where w_1 is the soil moisture in the upper layer, and w_{wp1} is the amount of soil moisture at wilting point. Further, w_{crit1} is the water moisture below when plants start to close their stomata (Van Der Knijff et al., 2010). Critical soil moisture is then calculated as:

$$w_{crit1} = (1 - p) \cdot \left(w_{fc1} - w_{wp1}\right) + w_{wp1}$$ (11)

with w_{fcl} as the amount of soil moisture at field capacity, and *p* being the water depletion fraction in the soil. Actual transpiration is further calculated as:

$$T_a = r_{ws} \cdot T_{max}$$ (12)

To compute the maximum amount of evaporation from the soil surface, the maximum evaporation from soil surfaces is computed in the equation:

$$ES_{max} = ES0 \exp\left(-\kappa_{gb}LAI\right)\Delta t$$ (13)

With *ES0* being the rate of potential evaporation rate from bare soil surfaces. Further, since actual evaporation from soil is dependent on the amount of soil moisture near the soil surface, i.e. since evaporation decreases as the topsoil dries, the LISFLOOD model simulates this process with a reduction factor in the equation:

$$ES_a = ES_{max}\left(\sqrt{D_{slr}} - \sqrt{D_{slr}-1}\right)$$

(14)

which is a function of the number of days since the last rain storm (Van Der Knijff et al., 2010). In this equation, the variable D_{slr} represents the number of days since the last rainfall. If the amount of water available for infiltration (W_{av}) is below a critical threshold, D_{slr} increases over time by the change in temperature per time step. If the critical amount of water is exceeded, the model sets D_{slr} to 1. Actual soil evaporation is calculated as a result of the previous equation, and is taken as the smallest value and the available moisture in the soil:

$$ES_a = min(ES_a, w_1 - w_{r1})$$

(15)

with w_1 being moisture in the upper soil layer, and w_{r1} being residual soil moisture (Van Der Knijff et al., 2010).

Infiltration capacity of soil in the model is estimated using the Xinanjiang method. This method considers sub-pixel heterogeneity of infiltration capacity, which is especially important when modeling large-scale runoff. This method assumes that the fraction of a grid cell that contributes to surface runoff is related to the total amount of soil moisture, which is calculated through a non-linear distribution function:

$$A_s = 1 - \left(1 - \frac{w_1}{w_{s1}}\right)^b$$

(16)

where A_s is the saturated fraction of a pixel, and w_{s1} and w_1 are the maximum and actual amounts of moisture in the superficial (1a) and upper (1b) soil layers respectively, and *b* is a dimensionless empirical shape parameter, usually used as a calibration constant (*LISFLOOD Model Documentation*, n.d.; Van Der Knijff et al., 2010). A_s is also expressed as a fraction of the pervious fraction, and thus the infiltration capacity INF_{pot} is a function of w_{s1} and A_s in the equation:

$$INF_{pot} = \frac{w_{s1}}{b+1} - \frac{w_{s1}}{b+1}\left[1 - (1 - A_s)^{\frac{b+1}{b}}\right]$$

(17)

Failing to account for preferential flow may lead to unrealistic model behavior during extreme rainfall, and thus the following equation is used within the LISFLOOD model:

$$D_{pref,gw} = W_{av} \left(\frac{w_1}{w_{s1}} \right)^{c_{pref}} \tag{18}$$

with $D_{pref,gw}$ being preferential flow per time step, and W_{av} being the amount of water available for infiltration. C_{pref} is another empirical shape parameter, which is used as a calibration constant. This equation then produces preferential flow that becomes important as water intake increases in the soil (Van Der Knijff et al., 2010). Actual infiltration can then be calculated as:

$$INF_{act} = \min \left(INF_{pot}, W_{av} - D_{pref,gw} \right) \tag{19}$$

 which can then be used in the equation for surface runoff (see equation 7).

Soil moisture flow is simulated within the model using Darcy's law for one-dimensional vertical flow. This is computed as:

$$D = -K(\theta) \left[\frac{\partial h(\theta)}{\partial z} - 1 \right] \tag{20}$$

Where D is the moisture flux out of a soil layer, i.e. the upper and lower soil layers, $K(\theta)$ is the hydraulic conductivity, θ is the soil's volumetric moisture content, and the remaining is the matric potential gradient. If matric potential gradient is assumed to be zero, then the flow in equation (20) is always in a downward direction, at a rate that is equal to the conductivity in the soil. Hydraulic conductivity and soil moisture status are further related in the Genuchten equation, which is written in terms of a water slice in the LISFLOOD model. It is used to calculate the fluxes from the upper to lower soil layers, and then from the lower soil layer to the groundwater:

$$D = K(w) = K_s \left(\frac{w - w_r}{w_s - w_r} \right)^{1/2} \left\{ 1 - \left[1 - \left(\frac{w - w_r}{w_s - w_r} \right)^{1/m} \right]^m \right\}^2 \tag{21}$$

where K_s is the saturated conductivity, w, w_r, and w_s are the actual, residual, and maximum amounts of moisture in the soil respectively. m is a parameter which is

calculated from the pore size index, and is related to soil texture in the following equation:

$$m = \frac{\lambda}{\lambda + 1} \tag{22}$$

For subsurface flow the LISFLOOD model contains a quick-runoff component for the upper zone, which includes a fast groundwater and subsurface flow through maco-pores in the soil. The lower zone represents slow groundwater that generates base flow. Outflow from the upper zone is calculated as:

$$Q_{uz} = \frac{1}{T_{uz}} \cdot UZ\Delta t \tag{23}$$

With Q_{uz} being the outflow from the upper zone, T_{uz} being the reservoir constant in days, and UZ being the water amount that is stored in the upper zone (Van Der Knijff et al., 2010). Additionally, the outflow from the lower zone is calculated as:

$$Q_{lz} = \frac{1}{T_{lz}} \cdot LZ\,\Delta t \tag{24}$$

Where Q_{uz} is the outflow from the lower zone, T_{lz} is the reservoir constant, again in days, and LZ is the water stored in the lower zone(Van Der Knijff et al., 2010). A fixed amount of water also percolates from the upper zone to the lower zone, which is calculated as:

$$D_{uz,\,lz} = \min\left(GW_{perc} \cdot \Delta t,\ UZ\right) \tag{25}$$

where GW_{perc} is a user-defined value that can be used as a calibration constant. The following equation was not simulated within the model because the lower groundwater zone was treated as a system with a completely closed boundary, however if the outflow from the lower zone is treated as a loss, it is calculated within the model using:

$$D_{loss} = f_{loss}(Q_{ls}) \tag{26}$$

In this equation, the loss term represents either water that is lost to deep groundwater systems that do not follow the catchment boundaries, or groundwater

extraction wells. The amount of water in the upper and lower zones are therefore updated for the in and out-going fluxes in the equations:

$$UZ_t = UZ_{t-1} + D_{2,\,gw} - D_{uz,\,lz} - Q_{uz} \tag{27}$$

$$LZ_t = LZ_{t-1} + D_{uz,\,lz} - Q_{lz} \tag{28}$$

The slow response to the lower zone is prone to initialization problems, thus the model can be run to calculate the steady-state of water storage for proceeding model runs (see section 3.4.1).

In terms of channel routing, there are two different components that the model considers. First, runoff from each pixel is routed to the nearest downstream channel. Then, the surface runoff is routed using a four-point implicit finite-difference solution of the kinematic wave equations from Chow et al. (1998). For sub-surface runoff, all water that flows out of the upper and lower groundwater zone is routed to the nearest downstream pixel within one time-step. Then, the water in each channel pixel is routed through the channel network, again using the four-point implicit finite-difference solution of the kinematic wave equations. The basic equations used are the continuity equation and the momentum equation. The continuity equation is:

$$\partial Qsr/\partial x + \partial Asr/\partial t = qsr \tag{29}$$

Where Q_{sr} is the surface runoff, A_{sr} is the cross-sectional area of the flow, and q_{sr} is the amount of lateral inflow per unit flow length (*LISFLOOD Model Documentation*, n.d.). The momentum equation is:

$$\rho \cdot g \cdot Asr \cdot (S0 - Sf) = 0 \tag{30}$$

where ρ is the density of the flow, g is the gravity acceleration, S_0 is the topographical gradient, and S_f is the friction gradient. For further documentation on the kinematic wave equations, see the LISLFOOD model documentation page (*LISFLOOD Model Documentation*, n.d.).

3.3 Data

As mentioned previously, the LISFLOOD-OS model is a GIS-based hydrological rainfall-runoff model, capable of simulating hydrological processes that occur in a catchment (Van Der Knijff et al., 2010). It is spatially distributed and based on raster files, which helps to simplify the large data requirements of the model (Cantoni et al., 2022). These data requirements include static maps and

meteorological forcings. The static maps provide the model with information on the underlying morphological, physical, soil, and land-use properties for each pixel within the catchment (*LISFLOOD User Guide*, n.d.). The meteorological forcings, which include precipitation, average temperature, and potential evapotranspiration time-series (specifically reference values for evaporation from open water bodies, bare soil, and a reference value of evapotranspiration), provide time series of values for each pixel within the catchment (Cantoni et al., 2022; *LISFLOOD User Guide*, n.d.). Meteorological data are required for each time step within the computational domain, and in this work included approximately 11,000 maps for each meteorological forcing respectively (*LISFLOOD User Guide*, n.d.).

3.3.1 Static Maps

Static maps were obtained at approximately 1 km spatial resolution. The static maps were developed using a variety of different data sources, however specifically from the sources and methodologies of CaMa-Flood, MERIT DEM, CORINE Land Cover 2018, Copernicus Global Land Cover Layers (CGLS), Global Lakes and Wetlands Database (GLWD), Spatial Production Allocation Model (SPAM), RiceAtlas, World Soil Information (ISRIC), Copernicus Global Land Service LAI Collection, SoilGrids250m (2017), FAO Irrigation and Drainage, and Open-Channel Hydraulics (*LISFLOOD Model Documentation*, n.d.).

The topography and channel geometry maps were prepared using data from CaMa-Flood and MERIT DEM. CaMa-Flood (Catchment-based Macro-scale Floodplain) is a model which was designed to simulate the hydrodynamics in continental-scale rivers (*CaMa-Flood*, 2021). Water levels and flooded areas are determined by the water storage at each unit-catchment, using sub-grid topographic parameters of the river channel and floodplains (*CaMa-Flood*, 2021). The model is driven by runoff forcing from a land surface model. Map data and sample input data were provided by the model developers, specifically by way of the global river map (river network map, river topography parameters, and high-resolution topography data, which were based on MERIT Hydro 1min resolution), preprocessed Eart2Observe (E2O) runoff products and runoff climatology data, and the river channel parameters (channel width and channel depth) (*LISFLOOD Model Documentation*, n.d.).

Land-use maps were prepared using data from CGLS and CORINE Land Cover 2018. The CGLS provides a Dynamic Land Cover map at 100m resolution which entails a primary land cover scheme, along with continuous field layers for basic land cover classes with proportional estimates for vegetation and ground cover (*Earth Engine Data Catalog*, n.d.). In terms of the LISFLOOD model, these maps provide the percentage of a grid-cell covered by a land-cover type (*LISFLOOD Model Documentation*, n.d.). The land-use maps were derived from the PROBA-V 100m timeseries, a database which reaches an accuracy of 80% at Level1 over all years (*LISFLOOD Model Documentation*, n.d.).

Land-use depending maps were prepared also using data from CGLS, the SPAM methodology., and SoilGrids250m. The SPAM methodology makes use of a cross-

entropy approach to make plausible estimates of crop distribution within disaggregated units (Harvard Dataverse, n.d.). SPAM provides estimates of crop distribution for 42 crops, such as cassava, potatoes, and wheat, and two production systems (irrigated and rainfed), which were input into the model to provide a spatial reference of crop production in the study area (*LISFLOOD Model Documentation*, n.d.). Further, the SoilGrids250m (2017) is a global collection of soil property class maps, which were produced using machine learning and statistical measures (*LISFLOOD Model Documentation*, n.d.)

Soil hydraulic property maps were prepared using data from ISRIC, which is an independent foundation that provides global soil information (*About ISRIC*, n.d.) . ISRIC data from 2020 were used in this work for a number of soil hydraulic property maps, such as clay, soil PH, and silt.

Leaf area index (LAI) maps were prepared using data from CGLS LAI Collection, Version 2, at 1km resolution. The product is derived from SPOT/VEGETATION and PROBA-V data (*LISFLOOD Model Documentation*, n.d.). Further documentation on the methodology for the preparation of LAI maps can be found on the LISFLOOD model documentation page.

Reservoirs and lakes maps were derived using data from the GLWD. These maps were produced in partnership with the World Wide Fund for Nature (*WWF*, 2004), the Center for Environmental Systems Research, and the University of Kassel, Germany, and provide data and information on lakes and wetlands on a global scale at 1:1 to 1:3 million resolution (*WWF*, 2004).

The rice calendar maps were produced using data from RiceAtlas, which is a spatial database for rice planting and harvesting dates by growing season, and estimates on monthly production for all rice-planting countries (Harvard Dataverse, n.d.). In cases where peak harvesting dates were not available, dates were estimated for the midpoint between start and end dates (*LISFLOOD Model Documentation*, n.d.).

3.3.2 Meteorological Forcings

As mentioned previously, the meteorological forcing data which is used in the model includes precipitation, P (mm day^{-1}), average temperature, T_{avg} (^{o}C), and evapotranspiration levels, including potential (reference) evapotranspiration rate of a closed canopy, $ET0$ (mm day^{-1}), potential (reference) evaporation rate from a bare soil surface, $ES0$ (mm day^{-1}), and potential (reference) evaporation rate from an open water surface, $EW0$ (mm day^{-1}) (Van Der Knijff et al., 2010). All meteorological data were obtained from the EMO-1 (European Meteorological Observations) dataset, which is a high-resolution, daily, multi-variable gridded meteorological dataset based on historical and real-time observations (*JRC Data Catalog*, n.d.). The EMO dataset is a Copernicus Emergency management service product, which provides daily data for total precipitation, minimum and maximum temperature, wind speed, solar radiation, and water vapor pressure. These data were put through a set of quality controls, and then underwent the SPHEREMAP and

Yamamoto interpolation methods in order to estimate variable value and uncertainty for each grid cell (*JRC Data Catalog*, n.d.).

Most meteorological datasets do not provide estimates of potential evaporation and evapotranspiration rates (Van Der Knijff et al., 2010), which was also found to be the case in this work. Thus, to obtain these values, the LISVAP model, a separate pre-processing application which was developed in conjunction with the LISFLOOD model, was used with meteorological data obtained from the EMO-1 dataset (Van Der Knijff et al., 2010). The LISVAP model uses the Penman-Monteith equation to calculate reference potential evaporation and evapotranspiration (Gai et al., 2019).

Meteorological data from 1990-2021 were prepared and run within the study area for the LISVAP model to obtain evapotranspiration and evaporation reference levels. Further, for the initialization period, meteorological data from 1990-2021 were also applied to the study area and prepared in map stacks to produce reasonable estimates of average discharge, as well as inflow into the lower groundwater zone (see further details in section 3.4.1). All meteorological data for the flooding event of 2021 and the future flooding scenario were prepared in map stacks for the years 2020-2021.

3.4 Model Set-up and Implementation

In terms of model set-up, Docker was used to connect local data files within the LISFLOOD-OS shell to run the necessary scripts for initialization, calibration, and the final model runs. Model code was extracted from Github via the LISFLOOD-OS Github page, with the settings files manipulated according to the Upper Rhine catchment requirements. The model was implemented to run a simulation according to discharge at the Mainz gauging station for comparison against observed data. All simulations were run at a daily time-step at 1 arcmin, or approximately 1 km spatial resolution, from January 1, 2020, through December 31, 2021. The time period chosen to run the model was done in order to provide a sufficient warm-up period to simulate the flooding event of 2021.

3.4.1 Initialization Run

An initial run, or initialization, is done to get the initial state of water stored in the catchment, so that proceeding model runs can produce reasonable water discharge (*LISFLOOD User Guide*, n.d.). Although a long warm-up period usually produces a reasonable initialization, the storage component in the model is dependent on the average residence time of water in it; essentially, while moisture content from the upper soil zone interacts with the meteorological forcing data almost immediately, the lower groundwater zone is very slow to respond to meteorological data; thus the average recharge (or steady-state storage) must be calculated, a value which is only known at the end of the simulation. This initialization run then produces an average discharge map, as well as lower zone average inflow, which provide these values on which the proceeding model runs can be based off of (*LISFLOOD User*

Guide, n.d.). In this work, the initialization was run for the years 1990-2021 within the study area to get a reasonable value for the steady-state storage of water in the Upper Rhine catchment.

3.4.2 Model Calibration

Uncertainties are possible unknowns regarding forcings in the model processes. These uncertainties could be caused by input data, or even the theory and methodology behind the model itself. To address these uncertainties, model calibration is therefore an important step to ensure that the model is implemented according to the catchment's specifications (Tom et al., 2022). More specifically, model calibration helps to find the most optimal parameter values, that is values which produce the best fit between the model simulation and historic observations of the catchment, measured in outputs such as water discharge (Ruijsch et al., 2021). The LISFLOOD model contains numerous parameters which can be calibrated, however most can be left to the model defaults made from prior estimates (Van Der Knijff et al., 2010). Thus, in this work a total of five parameters were calibrated, based on the calibration done by Feyen et al. (2007) for the Dutch-Belgian-French Meuse catchment. The parameters calibrated in this work include:

1. Upper zone time constant (T_{uz})
2. Infiltration constant (b)
3. Preferential flow constant (C_{pref})
4. Maximum rate of percolation from upper to lower zone (GW_{perc})
5. Lower zone time constant (T_{lz})

The Upper and Lower zone time constants represent the residence time of water in the upper and lower groundwater zones, respectively. These parameters affect the timing of outflow from groundwater reservoirs. The Groundwater Percolation parameter affects water flow from the upper to the lower groundwater zone. As referenced in equation 16, the Xinanjiang parameter, or infiltration constant, controls the infiltration capacity of the soil. This parameter controls the fraction of saturated area within a grid cell that contributes to runoff. Lastly, the Power Preferential Flow parameter relates water flow with the relative saturation of the soil (Feyen et al., 2007).

Feyen et al. (2007) chose these parameters to calibrate because they lack a physical basis that cannot be directly obtained by field data; due to the LISFLOOD model's lumped representation of some processes, these five parameters in particular need to be estimated against stream flow records (Feyen et al., 2007). Thus, for the purposes of this work these parameters were also calibrated.

The calibration approach used in this work was a manual calibration strategy, where the parameters implemented by Feyen et al. (2007) were iterated over model runs

with different values until the most optimal parameter combination set was obtained.

To quantify how well model simulations compared to observations, the Kling-Gupta efficiency (KGE) objective function was used. The KGE objective function is a robust approach within the literature of hydrological modeling (Cantoni et al., 2022; Gai et al., 2019; Hirpa et al., 2018; Knighton et al., 2020; Peredo et al., 2022; Ruijsch et al., 2021), and was therefore used in this work for the evaluation of modeled results. KGE can further be defined as:

$$KGE = 1 - \sqrt{\left(CC - 1\right)^2 + \left(\frac{cd}{rd} - 1\right)^2 + \left(\frac{cm}{rm} - 1\right)^2} \tag{30}$$

with KGE being a linear combination of three components of modeling error, specifically the Pearson correlation coefficient, the bias ratio, and variability ratio between observed and simulated runoff (Cantoni et al., 2022). KGE is a diagnostically interesting decomposition of the Nash-Sutcliffe efficiency (NSE), however due to the potential limitations of the NSE metric, KGE was used (Cantoni et al., 2022; *Agrimetsoft*, 2019). For a full description of the different components of the KGE metric, see Gupta et al. (2009).

3.5 Flood-Risk Analysis

3.5.1 EU Flood Depth-Damage Functions

The flood depth-damage functions for EU member states are risk functions based on economic measures, which assess damage for a given land-type based on water depth. The depth-damage functions were implemented in this work based on the water-depth output maps from the LISFLOOD simulations to quantify flood-risk in both the flooding of 2021 and a future flooding scenario. The EU flood depth-damage functions range from 0 to 1, with 0 being no damage incurred and a 1 being maximum damage. Further, these damage functions are separated by land use type, which was applied in this work regarding land-use types in Germany. The damage classification schemas produced by Huizing et al. (2007) can be seen in Tables 1, 2, 3 and 4.

As mentioned before, Dottori et al. (2017) implemented this risk methodology in their work to assess a rapid risk assessment procedure for Europe. Like Dottori et al. (2017), the outputs from LISFLOOD model simulations were used to compute the flood-risk assessment; specifically, separate flood depth-damage functions depending on land use type were applied to water depth output maps from LISFLOOD simulations. For land use classification, the land use types from the CORINE Land-Cover schema for Germany, 2018, were reclassified according to the land-use types for the EU depth damage functions: these land use classes were residential, industry, infrastructure, and agricultural areas. Since the output maps of

LISFLOOD simulations are in raster format, these outputs were vectorized. After water-depth maps were vectorized, the classification could be performed within a Python framework in a GIS to produce the final flood-risk maps. It must be noted that since the spatial resolution of the LISFLOOD simulations was approximately 1km, the vectorized water-depth data was taken as the nearest land-use class.

It must also be noted that although the LISFLOOD model can produce water-depth within a given grid-cell, the flood inundation extent of a flooding event is not simulated within the model. Thus, for the purposes of this work, flood-risk maps follow a more similar approach to Afsari et al. (2022), where final flood-risk maps containing a range of high and low risk values were produced according to the EU flood depth-damage functions produced by Huizinga et al. (2007).

Dottori et al. (2017) further compared their impact assessment maps against Copernicus Emergency Management Services (EMS) footprints to validate simulated flood extent, which was also done in this work regarding areas which were flooded. Areas which were classified within the flood depth-damage framework were compared against Copernicus EMS footprints to evaluate if flood-risk classified areas fell within areas which were flooded in 2021 within the study area.

Table 1. EU depth-damage function values for the residential land use class

Residential buildings	
Water depth (m)	Damage factor
0	0
0.5	0.25
1	0.4
2	0.5
3	0.6
4	0.75
5	0.85
6	0.95

Table 2. EU depth-damage function values for the industry land use class

Industry

Water depth (m)	Damage factor
0	0
0.5	0.15
1	0.27
1.5	0.4
2	0.2
3	0.7
4	0.85
5	1
6	1

Table 3. EU depth-damage function values for the infrastructure land use class

Infrastructure

Water depth (m)	Damage factor
0	0
0.5	0.25
1	0.42
1.5	0.55
2	0.65
3	0.8
4	0.9
5	1
6	1

Table 4. EU depth-damage function values for the agriculture land use class

Agriculture

Water depth (m)	Damage factor
0	0
0.5	0.3
1	0.55
1.5	0.65
2	0.75
3	0.85
4	0.95
5	1
6	1

3.5.2 Future Flooding Event Scenario

In their 6th assessment report on water cycle changes, the IPCC projected an increase in the magnitude of extreme precipitation to be approximately 7 percent for each 1°C of global warming. This is because air near Earth's surface can carry approximately 7% more water in its gas (vapor) for each 1°C warming; thus, a warmer climate increases the amount and intensity of rainfall during wet events, and this is expected to amplify the severity of flooding (IPCC, 2022). While the IPCC notes that this will also differ regionally, for the purposes of this work the precipitation values for the future flooding scenario were increased by 7 percent to simulate a higher-risk scenario of flooding. This higher-risk scenario was then compared against flood depth-damage classifications from 2021 to evaluate the changes in damage which would occur in this higher-precipitation flooding event.

Chapter 4

RESULTS

4.1 Model Calibration Results

From the manual calibration of the five parameters implemented by Feyen et al. (2007), the most optimal parameter values achieved can be seen in Table 5. The manual calibration was iterated over multiple simulations changing parameter values at increasing and decreasing values, to produce the final parameter values which were used to simulate the flooding event of 2021, as well as the future flooding scenario. The best KGE value which was achieved in the manual calibration was 0.438, which was a vast improvement over using the default parameter values, at a KGE of -4.343. Manual calibration discharge time series with their respective KGE values can be seen in the hydrograph in Figure 4. For simplification purposes not all model runs were included in Figure 4, however it gives an overview of the different KGE values which were obtained. All calibration simulations were run over the time of January 1, 2020-December 31, 2021.

Table 5. The parameters which were focused on for the manual calibration in this work, with the minimum, maximum, and default values as outlined in the LISFLOOD model documentation page (*LISFLOOD Model Documentation*, n.d.). The parameter values which achieved a KGE score of 0.438 were found with a manual calibration strategy.

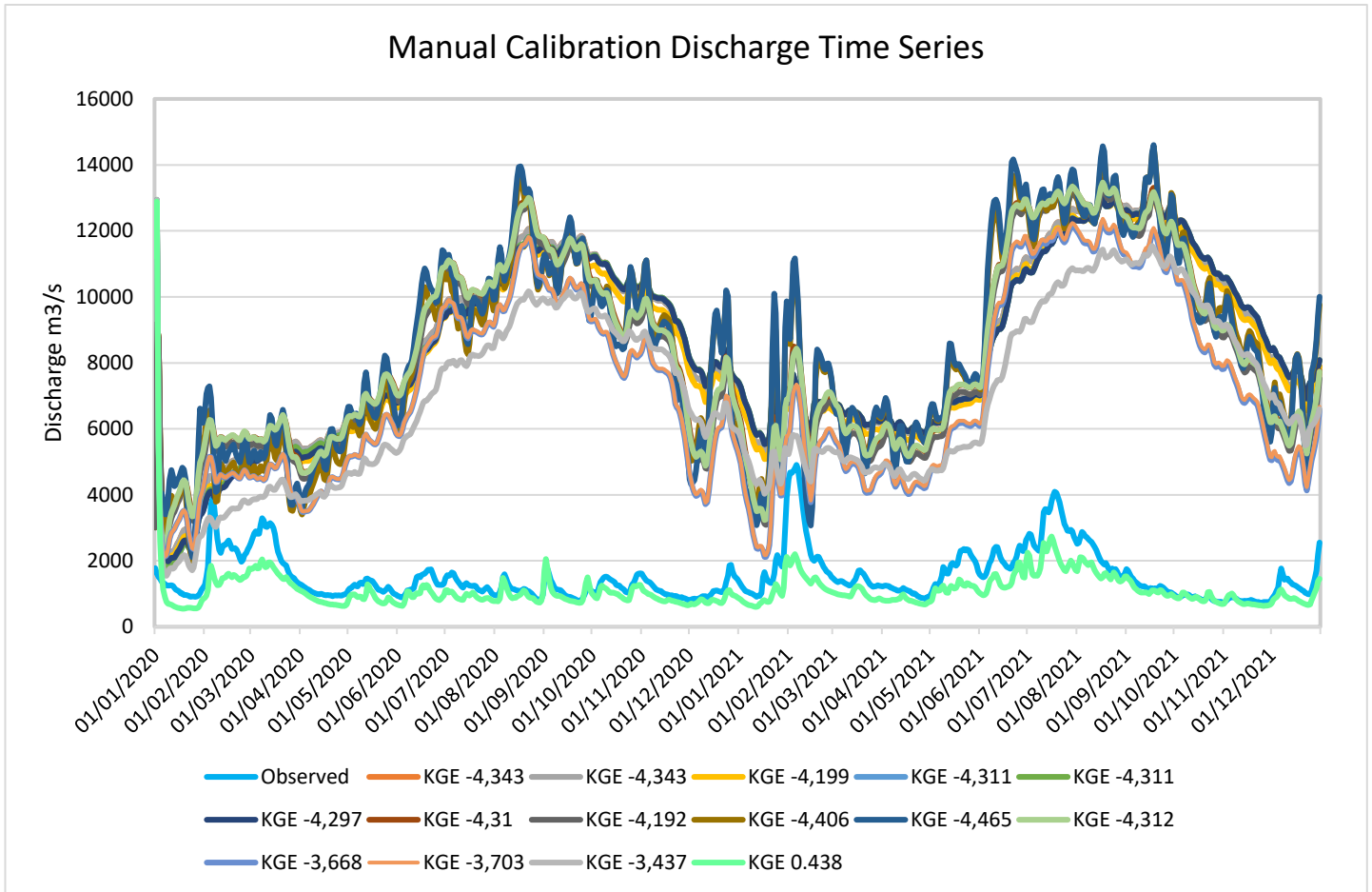| Parameter	Minimum	Maximum	Default	Optimal
Upper Zone Time Constant	0.01	40	10	35
Lower Zone Time Constant	40	10000	100	10000
Groundwater Percolation	0.01	2	0.5	2
Xinanjiang	0.01	5	0.5	0.5
Power Preferential Flow	0.5	8	4	4
KGE			-4.343	0.438

Fig. 4 Manual calibration runs with respective KGE values, shown against observed water discharge values from the Mainz gauging station. The best KGE score which was obtained during model calibration was 0.438.

4.2 Flooding of 2021 Simulation Result

After the initialization run and model calibration, the simulation for the flooding event of 2021 was completed using calibrated parameter values to produce reasonable water discharge values. At its peak during the flooding event, simulated discharge was equal to 970.038mm on July 15, 2021. Observed water discharge recorded at the Mainz gauging station during July 15, 2021, was 1280mm. Simulated values were thus relatively lower than observations, and produced a KGE score of 0.438. The hydrograph in Figure 5 shows the observed discharge values compared against the modeled result for the flooding event of 2021. From this hydrograph, the water discharge peaks follow a similar curve compared to observed discharge, showing that the parameter values were reasonable for the Upper Rhine catchment.
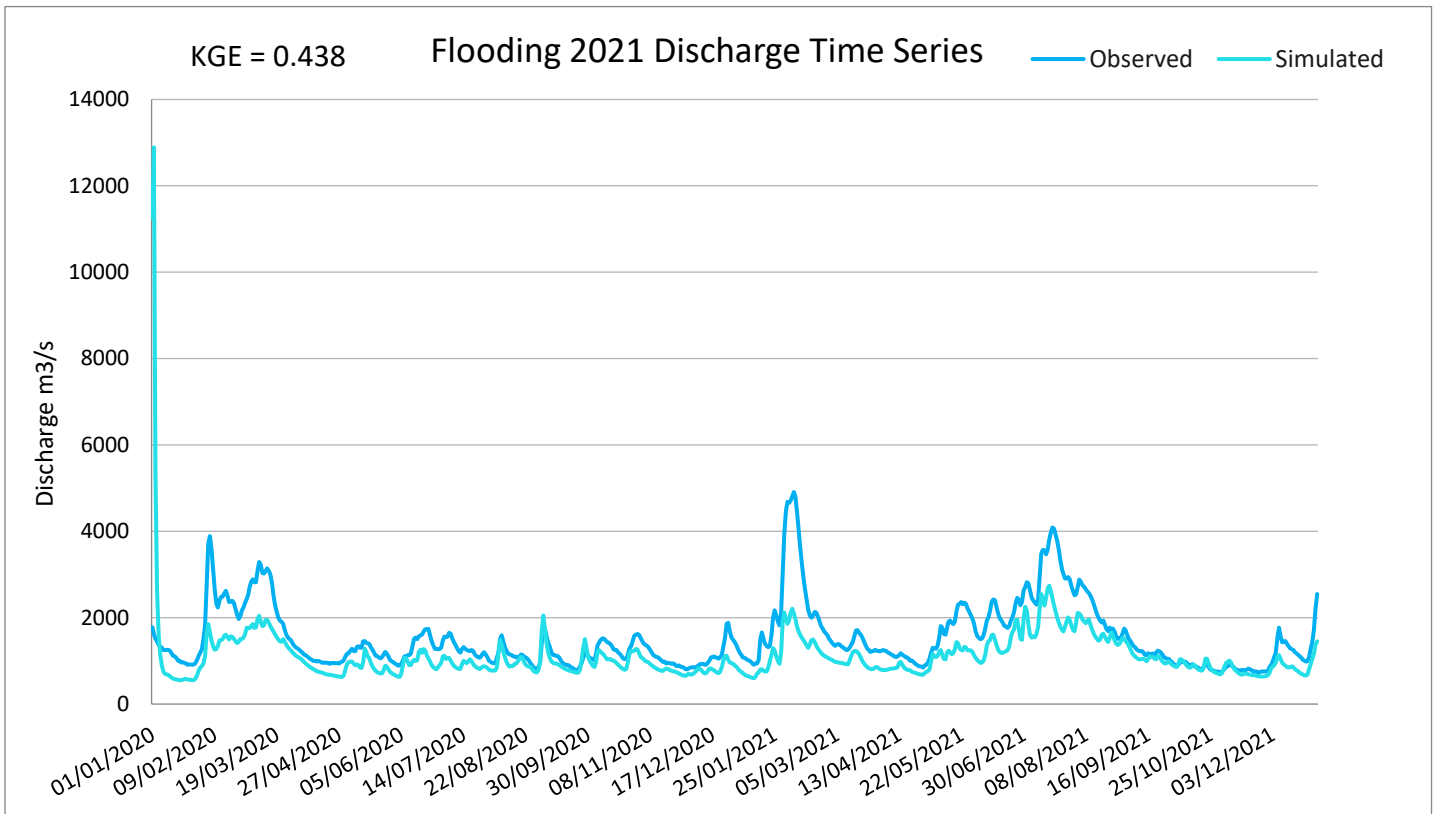
Fig. 5 Water discharge time series for the flooding event of 2021, with modeled simulations compared to observations from the Mainz gauging station.

4.3 Flooding of 2021 Flood Risk Analysis

In terms of the flood risk which incurred in the flooding event of 2021, as mentioned previously the EU flood depth-damage functions were applied according to each land use type in the classification to produce the final classification maps for the flooding event, seen in Figures 6 and 7.

Within the Moselle River area, the land use type which received the highest damage values were agricultural areas, with values ranging from 0.3-0.65. The next land use class which received the highest amount of damage were residential areas, receiving values ranging from 0.25-0.6. Industrial areas received relatively low damage, ranging from 0-0.27, and infrastructural areas received no damage. It can be seen in Figure 6 that the LISFLOOD model simulation was able to capture flooded areas which were recorded by Copernicus, namely agricultural and residential areas by the river.

For Bad Neuenahr-Ahrweiler, the land use class which received the most damage according to the flood-risk classification was also agricultural areas, receiving

damage values ranging from 0.3-0.75. The land use class which received the second most damage was residential areas, receiving damage values ranging from 0.4-0.6. Industrial areas did not receive any damage according to the flood-risk classification, and infrastructure received some damage, ranging from 0-0.65; although it can be seen that these areas are outside the Copernicus monitored flood areas. As mentioned previously, since LISFLOOD simulations were done with approximately 1 km spatial resolution, vectorized water-depth data was taken as the nearest land-use class; thus, some areas outside the river area were classified as having water depth. Nevertheless, areas near the river did receive some of the highest damage values which can be seen in Figure 7.

For further visualization of the flood-risk classification, Figures 8 and 9, show high and low risk areas for all land use types according to their respective damage levels. For Bad Neuenahr-Ahrweiler (Fig. 9), areas near Copernicus monitored flood areas for the flooding event were classified as moderately-high to high risk; albeit, some areas outside of the flooding area were classified as high-risk as well, which will be discussed in the limitations (see section 5.1.2). For the Moselle River area (Fig. 8), a similar pattern can be seen as areas near the river were classified as moderately-high to high risk.
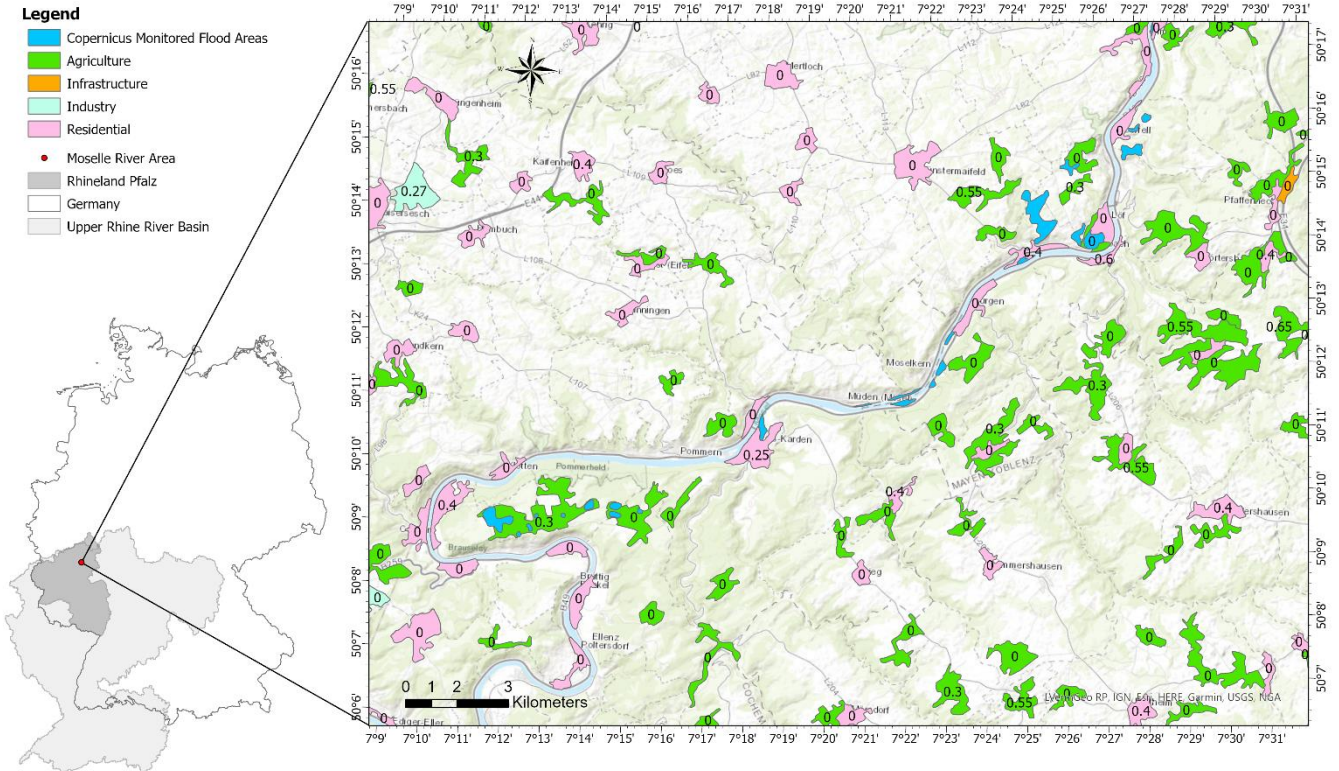
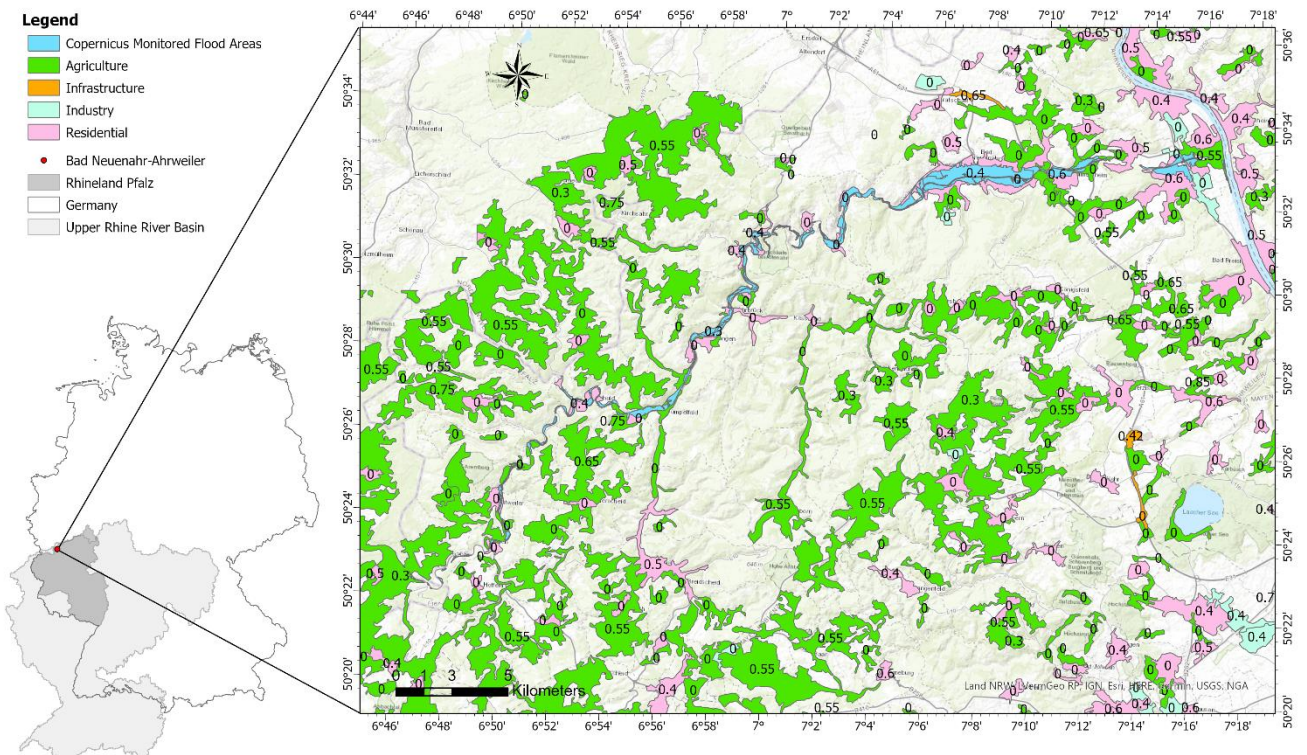**Fig 6.** Flood risk analysis for the flooding event of 2021 in the Moselle River area.

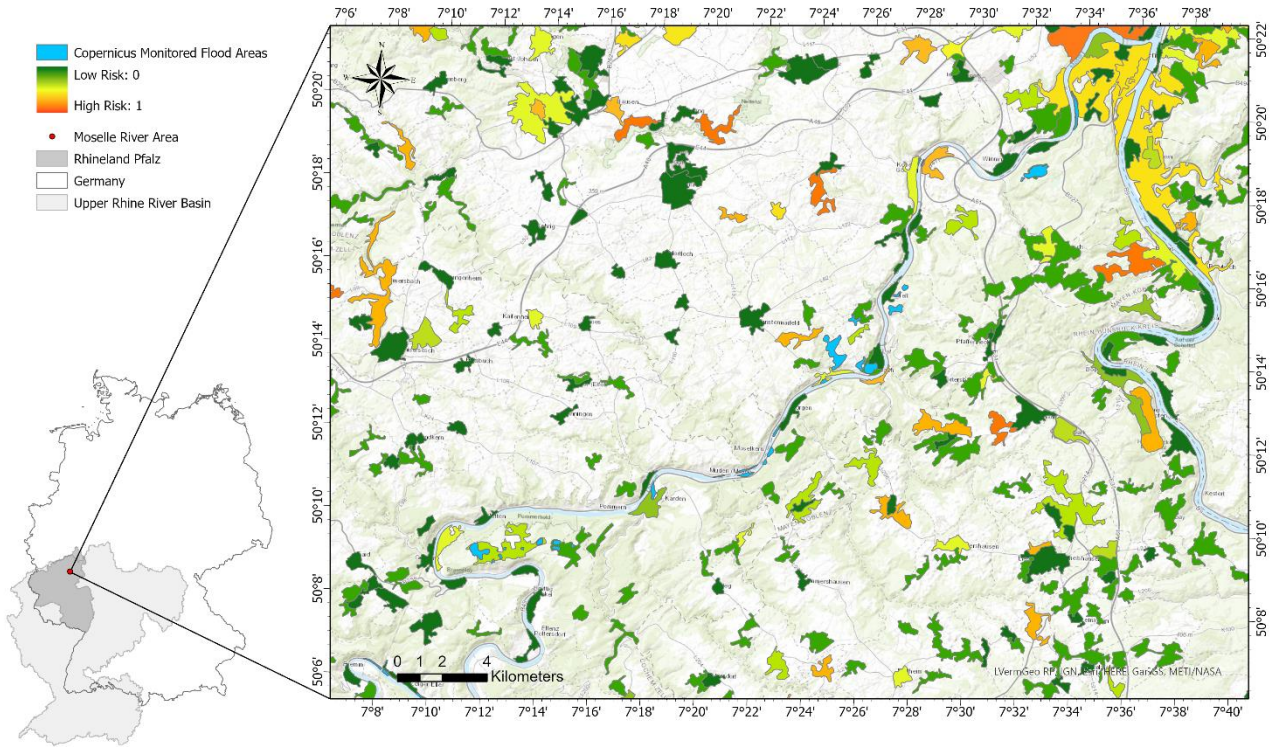**Fig. 7** Flood risk analysis for the flooding event of 2021 in Bad Neuenahr-Ahrweiler

Fig. 8 Combined flood risk classification of all land use classes in their respective damage schemas for the Moselle River area, in the flooding event of 2021.
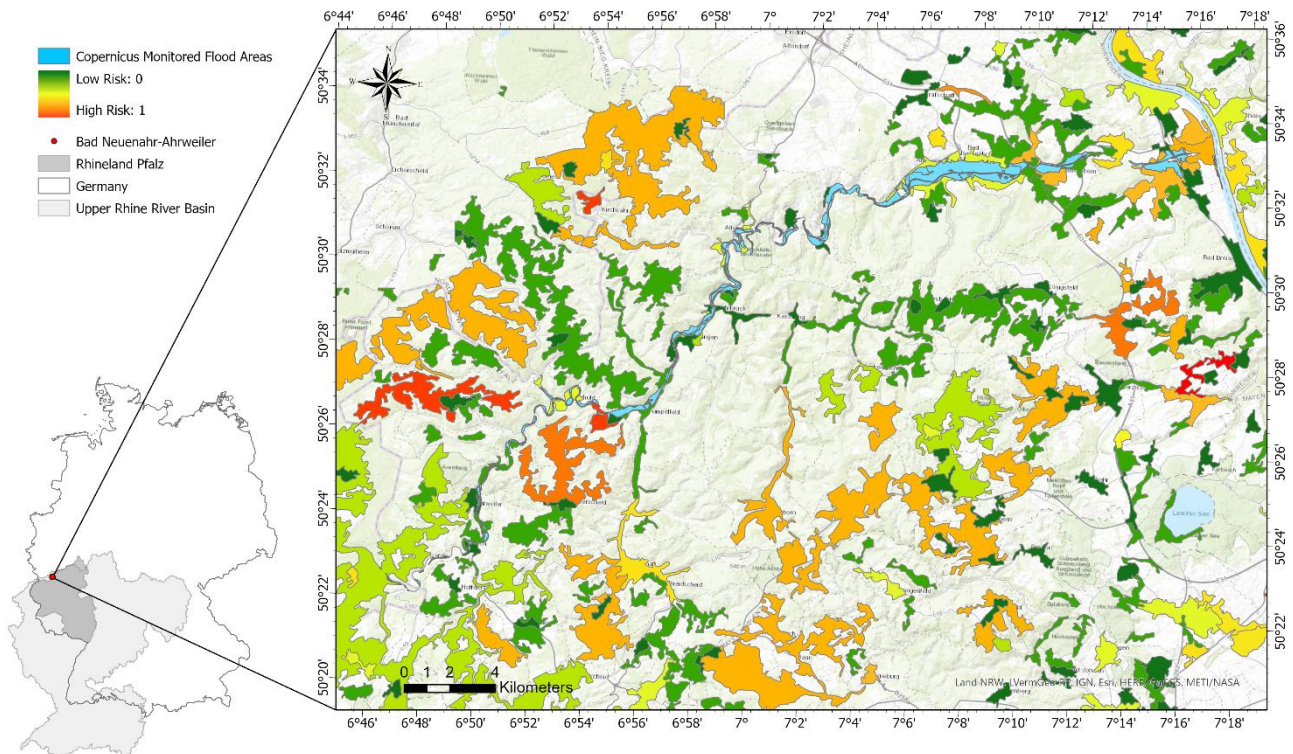

Fig. 9 Combined flood risk classification of all land use classes in their respective damage schemas for Bad Neuenahr-Ahrweiler, in the flooding event of 2021.

4.4 Future Flooding Event Scenario Result

In a future flooding scenario, with a 7 percent increase in precipitation, the Moselle River area would receive 2670.85mm of precipitation for the same timestep as the flooding event of 2021. This equates to 372.59mm more water discharge compared to the flood simulation on July 15, 2021. The hydrograph in Figure 10 shows the simulated water discharge levels for this future flooding scenario compared to simulated discharge levels from 2021. The calibrated parameter values were kept constant for the future flooding scenario.
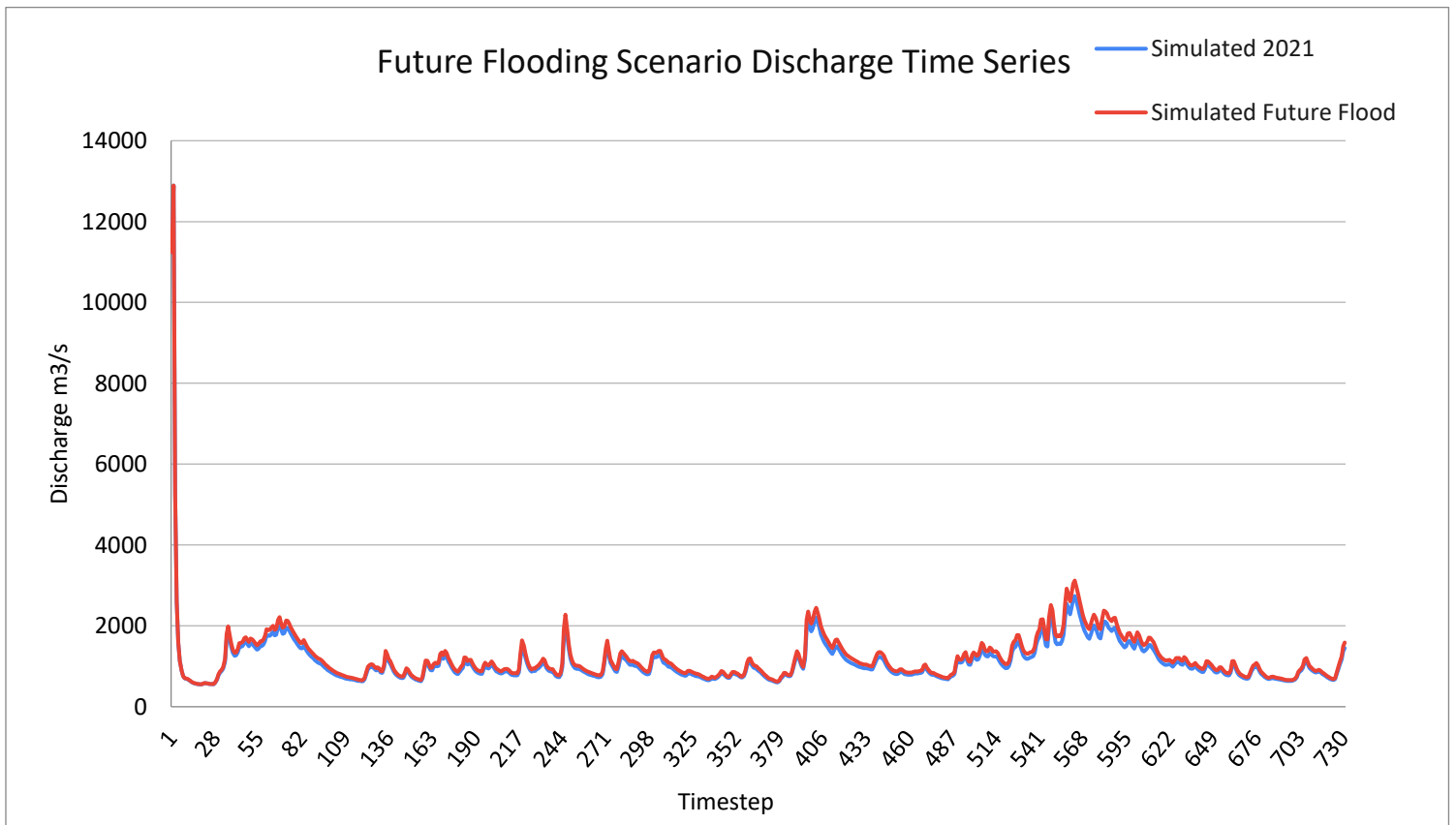

Fig. 10 Future flooding scenario water discharge time series, implemented by increasing precipitation by 7 percent.

4.5 Future Flooding Event Flood Risk Analysis

In terms of risk that would incur in this future flooding scenario, within the Moselle River area (Fig. 11), areas classified as agricultural and residential would experience the most damage, with values ranging from 0.3-0.65 and 0.25-0.75 respectively. While agricultural areas received the same amount of risk in the future flooding scenario, residential areas received a higher amount of risk, increasing from 0.6 to 0.75. Industrial areas also received the same amount of damage, ranging from 0-0.27, and infrastructure again received no damage.

Similar to the Moselle River area, areas classified as agricultural and residential within Bad Neuenahr-Ahrweiler (Fig. 12) also would receive the highest levels of damage, ranging from 0.3-0.75 and 0.4-0.75 respectively. Industrial areas would receive damage ranging from 0-0.4, and infrastructural areas ranging from 0.42-0.65. Thus, agricultural areas in a future flooding scenario received the same amount of damage as the flooding event of 2021, while residential, industrial, and the lower-bound of damage for infrastructural areas, all increased in damage values.

High and low risk classifications for all areas with their respective damage value schemas were visualized in Figures 13 and 14; in terms of future FRM practices that should be implemented to prepare for another pluvial flooding event, these areas could be focused on to reduce future flood impacts.
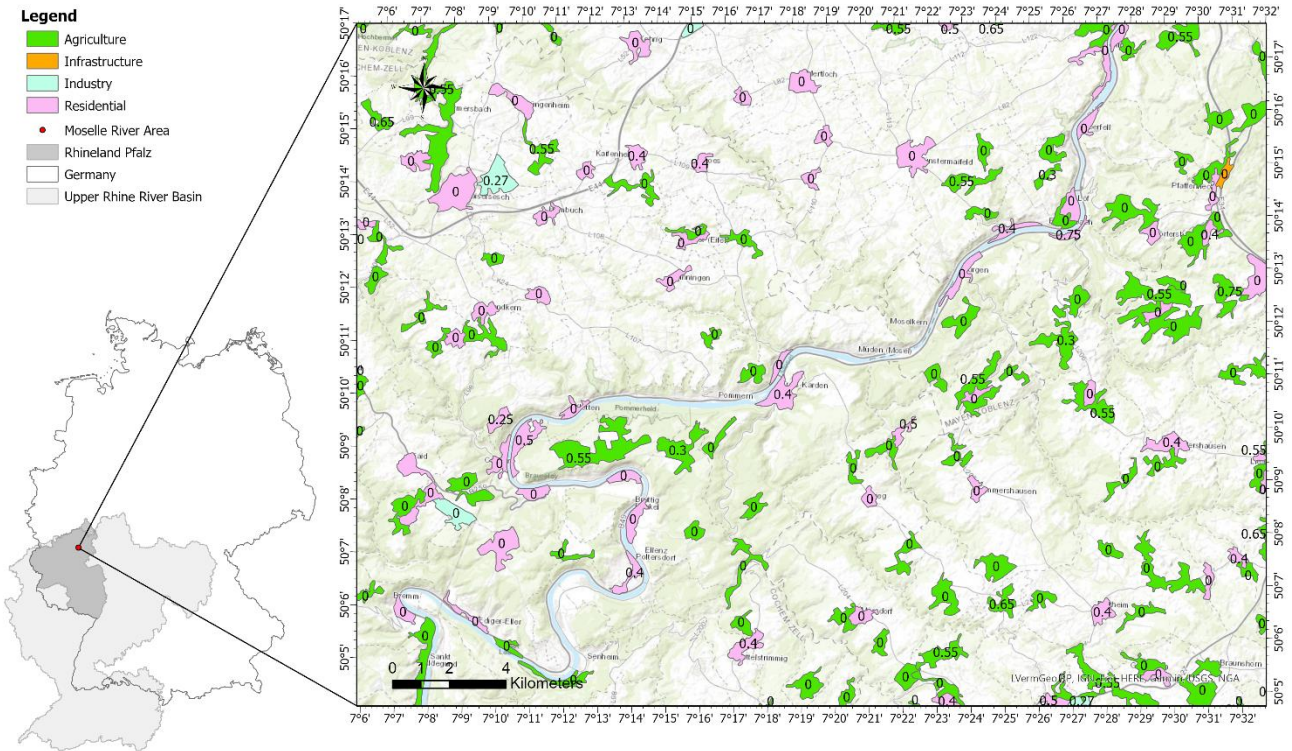
Fig. 11 Flood risk analysis for a future flooding scenario in the Moselle River area.
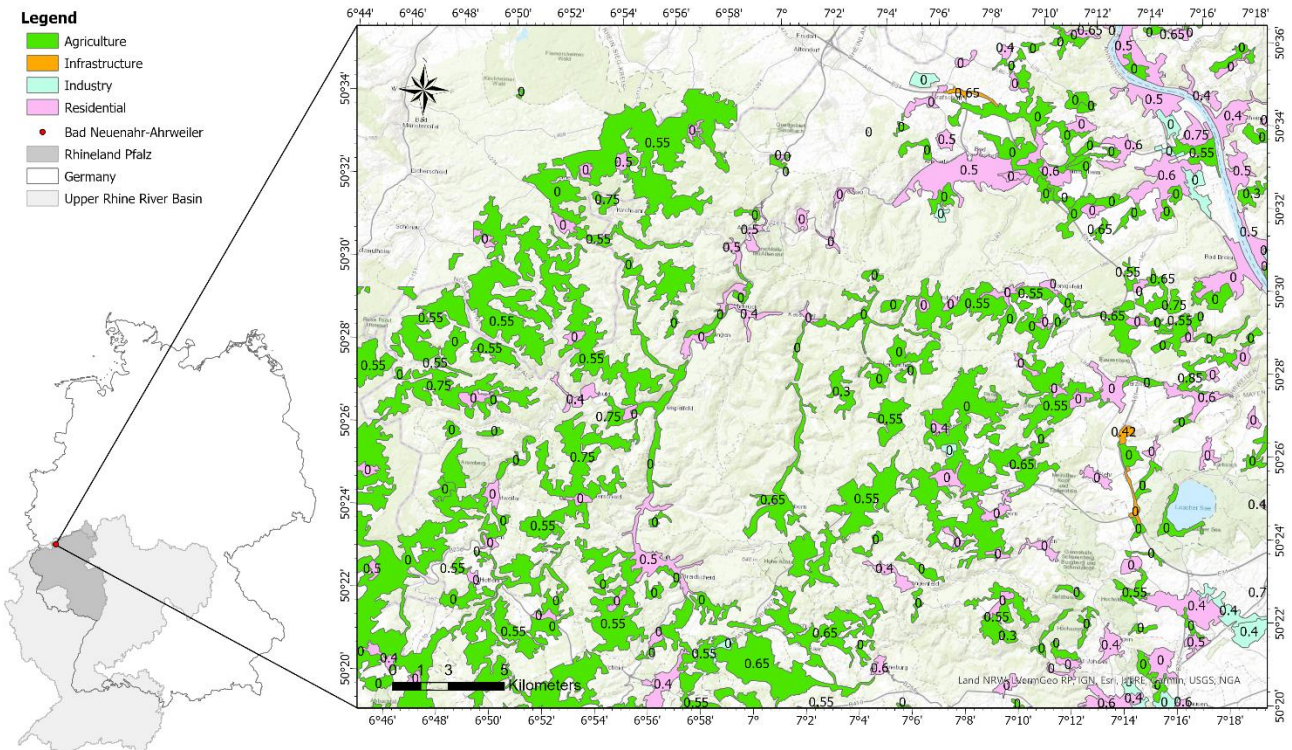

Fig. 12 Flood risk analysis for a future flooding scenario in Bad Neuenahr-Ahrweiler.
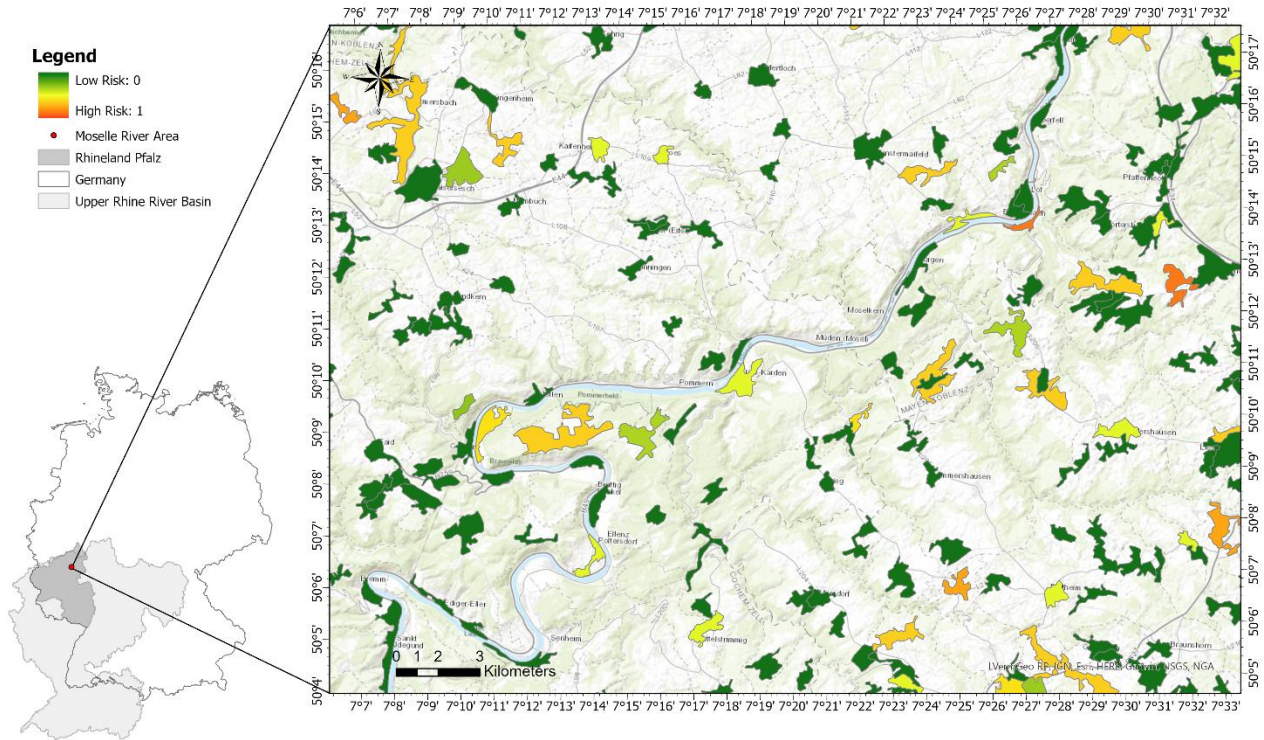
Fig. 13 Combined flood risk classification of all land use classes in their respective damage schemas for the Moselle River area, in a future flooding scenario.
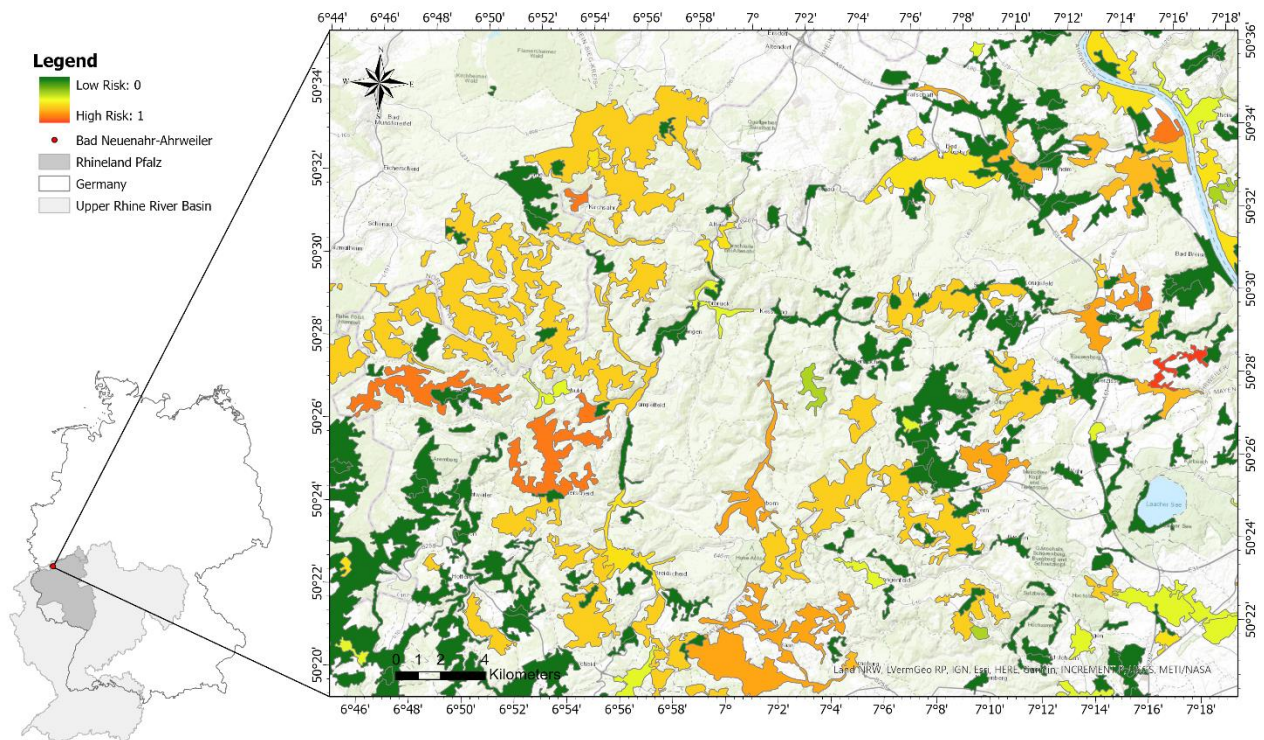

Fig. 14 Combined flood risk classification of all land use classes in their respective damage schemas for Bad Neuenahr-Ahrweiler, in a future flooding scenario.

Chapter 5

DISCUSSION AND CONCLUSION

5.1 Discussion

Transferring flood simulations into flood-risk remains a broad field with limited applications. While there are numerous hydraulic and hydrological models with different capabilities depending on the study aim, the LISFLOOD-OS model was chosen in this work for its ability to simulate hydrological processes in large European basins (Dottori et al., 2017; Feyen et al., 2007; Hirpa et al., 2018; Shustikova et al., 2019). Many other studies also found that calibration of the LISFLOOD model improved simulations (Cantoni et al., 2022; Feyen et al., 2007; Gai et al., 2019; Hirpa et al., 2018) which was also found in this work.

Results showed that the manual calibration strategy employed in this work was able to improve simulations to a KGE score of 0.438. Compared to the model default parameter values, which produced a KGE of -4.343, model calibration greatly improved simulated streamflow. The calibration result in this work is comparable to other studies which also used the LISFLOOD model and the KGE as the objective function. For example, through usage of the DEAP calibration strategy, Gai et al. (2019) achieved a KGE value of 0.85 in their calibration of the LISFLOOD model in the Wei River Basin, China. Also using the DEAP algorithm, Cantoni et al. (2022) achieved a KGE score of 0.48 in their calibration of the LISFLOOD model for catchments located in Tunisia, North Africa. Hirpa et al. (2018) achieved a median KGE score of 0.15 across all basins using the DEAP algorithm in their global calibration of the Global Flood Awareness System (GloFAS), which utilizes the LISFLOOD model. While perfect agreement between observations and simulations would produce a KGE score of 1, as noted by Cantoni et al. (2022), a KGE of -0.41 is the value corresponding to a mean flow benchmark. Thus, a KGE score of 0.438 produced in this work means that the model was able to simulate water discharge levels close to reality.

While other works applied the DEAP algorithm with the LISFLOOD model (Cantoni et al., 2022; Gai et al., 2019; Hirpa et al., 2018; Knighton et al., 2020; Peredo et al., 2022; Ruijsch et al., 2021), the calibration strategy applied in this work was nonetheless able to find parameter values which were reasonable for the Upper Rhine catchment. Furthermore, the results from the calibration affirm that the parameters which were calibrated by Feyen et al. (2007) in the Dutch-Belgian-French Meuse catchment could also apply to the Upper Rhine catchment.

Most studies found within the literature which used the LISFLOOD model focused on model calibration; although this was not the main focus of this work, it was still a vital component to ensure that model simulations were correctly implemented according to the Upper Rhine Catchment. In this way, successful model calibration

helps to validate that the simulation outputs used in the flood-risk analysis were reliable. In truth it is difficult to transfer streamflow data into flood-risk; while Dottori et al. (2017) used flood forecast data in their risk assessment for Europe, this work is novel in that it uses the LISFLOOD model in combination with the EU flood depth-damage functions in a classification schema. By drawing on methodologies employed by other flood-risk assessments (Afsari et al., 2022), this work presents a way to classify flood-risk by taking into account flood damage functions, which are an important element for flood damage assessment and impact studies (Huizinga, 2007).

The flood-risk methodology demonstrated in this work was able to show land-use classes which were impacted in the flooding event of 2021, as well as in a future flooding scenario. Interestingly, damage values changed in a future flooding scenario depending on land use class. Namely, for the Moselle River area, while agricultural, industrial, and infrastructure areas received the same amount of risk, residential areas received a higher amount of risk. For Bad Neuenahr-Ahrweiler, agricultural areas in a future flooding scenario remained the same in terms of damage values, while residential, industrial, and the lower-bound of damage for infrastructural areas, all increased in damage values. This shows that flood-risk changes differentially for land use classes, and highlights the importance of taking into account spatial differences when quantifying risk. As noted by Afsari et al. (2022), vulnerability is highly dependent on environmental conditions and contexts, with differing outcomes of vulnerability being attributed to spatial distinctions; from the differing amounts of risk that incurred depending on land use class in a future flooding scenario, this was supported by the results of this work.

5.1.1 Limitations

It must be noted that this work was limited in several different aspects. Firstly, even though the manual calibration strategy resulted in a KGE score of 0.438, water discharge levels for the flooding event of 2021 were still underestimated by the model. Although a KGE score of 0.438 indicates that the model was able to produce reasonable discharge levels, simulated impacts will always be different from actual impacts (Dottori et al., 2017). Model underestimations for the flooding event of 2021 and the future flooding event scenario therefore must be considered as a limitation of this work.

Secondly, the spatial resolution of input data was also a limitation in this work. Since the input data for both static maps and meteorological forcings was approximately 1km spatial resolution, this means that for smaller-scale areas such as the Moselle River area and Bad Neuenahr-Ahrweiler, simulated outputs did not perfectly align with smaller-scale land use classes. Even though simulated outputs were able to capture areas which were flooded in 2021, this is an obvious limitation as areas outside of flooded areas were also classified as having water depth, and thus having damage values. While the LISFLOOD model is able to simulate data at any spatial resolution, using higher spatial resolution data was not feasible in this

work, because there is not currently readily available data at a finer resolution for the static inputs that the LISFLOOD model requires.

5.1.2 Further Applications

As it was a limitation, increasing the spatial resolution of input data, in terms of static maps and meteorological forcings, could be an avenue of further development. Increasing the spatial resolution of input data would enable the simulation of the flooding event on at a finer scale, and possibly improve the accuracy of the risk quantification. While the creation of static input maps is a very complex process, the creation of these higher-resolution data could create many more opportunities of use-cases with the LISFLOOD model, especially in simulating flooding and flooding events which may occur in smaller study areas.
Another application could be to use the LISFLOOD-FP model in combination with the LISFLOOD-OS model. While other literature sources also employed the LISFLOOD-FP model (Knighton et al., 2020; Shustikova et al., 2019), in this work only the LIFLOOD-OS model was used for flood simulation. Use of the LISFLOOD-FP model could also prove to be advantageous, however, especially in simulating flood extent.

In terms of the flood-risk quantification, another interesting application mentioned by Dottori et al. (2017) would be to use LISFLOOD-OS model simulations to determine the effects that flooding events may have on human life, specifically by calculating probabilistic risk methods by using mortality rates from previous flood events. This application could also be useful for policy makers, and add to the risk-quantification, to not only see areas which would be affected by a future flooding event, but also how many lives could be in danger.

5.2 Conclusion

Due to climate change and urban growth, extreme flooding events are occurring more frequently on a global scale (Gai et al., 2019; Surminski & Thieken, 2017). This means that populations which live in flood-prone areas are in need more than ever of flood mitigation and management efforts. This work presented the application of a flood-risk quantification approach using the LISFLOOD-OS model in the Upper Rhine River basin. Through flood simulation and risk classification, flood-risk maps provide residents and governments a classification of damages that occurred in the flooding event of 2021 in the Rhineland Pfalz region, as well as the damages that may incur with higher levels of precipitation for the same region. Results showed that the flooding event of 2021 could be modeled with reasonable discharge levels compared to observations from the Mainz gauging station, producing a KGE score of 0.438. Further, land use classes which received the highest damage values in both the simulated flooding event of 2021 and in the future flooding event scenario were agricultural and residential areas. Damage values between the flooding of 2021 and a future flooding scenario changed depending on land use class, showing the importance of spatial distinctions when quantifying risk. While the flood-risk maps may serve as a way to show areas which

could be at high-risk in a future flooding scenario, these maps should not be used for any final decision-making purposes. As noted by Dottori et al. (2017), the present methodology would need to undergo an accurate uncertainty analysis before the risk assessments could be used for emergency management.

Nonetheless, the present work demonstrates an application of the LISFLOOD model with a flood-risk quantification approach that has the potential to be used in future planning efforts, namely, to help reduce the impacts of large-scale flooding events. Since flooding events can strike at any time, it is important to be able to identify where to focus flood mitigation efforts; the flood-risk analysis in this work thus showcases one possible way to identify high-risk areas, which could be focused on for FRM practices. Considering that pluvial floods have largely been neglected in Germany (Surminski & Thieken, 2017), flood simulations and the quantification of risk could be advantageous not only in reducing economic losses, but also in saving human lives.

References

Afsari, R., Nadizadeh Shorabeh, S., Kouhnavard, M., Homaee, M., & Arsanjani, J. J. (2022). A Spatial Decision Support Approach for Flood Vulnerability Analysis in Urban Areas: A Case Study of Tehran. *ISPRS International Journal of Geo-Information*, *11*(7), Article 7. https://doi.org/10.3390/ijgi11070380

Ajjur, S. B., & Al-Ghamdi, S. G. (2022). Exploring urban growth–climate change–flood risk nexus in fast growing cities. *Scientific Reports*, *12*(1), Article 1. https://doi.org/10.1038/s41598-022-16475-x

Bosseler, B., Salomon, M., Schlüter, M., & Rubinato, M. (2021). Living with Urban Flooding: A Continuous Learning Process for Local Municipalities and Lessons Learnt from the 2021 Events in Germany. *Water*, *13*(19), Article 19. https://doi.org/10.3390/w13192769

CaMa-Flood: Global River Hydrodynamics Model. (2021, March 31). CaMa-Flood: Global River Hydrodynamics Model. http://hydro.iis.u-tokyo.ac.jp/~yamadai/cama-flood/index.html

Cantoni, E., Tramblay, Y., Grimaldi, S., Salamon, P., Dakhlaoui, H., Dezetter, A., & Thiemig, V. (2022). Hydrological performance of the ERA5 reanalysis for flood modeling in Tunisia with the LISFLOOD and GR4J models. *Journal of Hydrology: Regional Studies*, *42*, 101169. https://doi.org/10.1016/j.ejrh.2022.101169

Chow, V. T., Maidment, D. R., & Mays, L. W. (1998). *Applied Hydrology*. McGraw-Hill Book Company. https://ion.sdsu.edu/Applied_Hydrology_Chow_1988.pdf

Copernicus Global Land Cover Layers: CGLS LC100 Collection 3. (n.d.). Earth Engine Data Catalog. https://developers.google.com/earth-engine/datasets/catalog/COPERNICUS_Landcover_100m_Proba-V-C3_Global#description

Dottori, F., Kalas, M., Salamon, P., Bianchi, A., Alfieri, L., & Feyen, L. (2017). An operational procedure for rapid flood risk assessment in Europe. *Natural Hazards and Earth System Sciences*, *17*(7), 1111–1126. https://doi.org/10.5194/nhess-17-1111-2017

El-Saoud, W. A., & Othman, A. (2022). An integrated hydrological and hydraulic modelling approach for flash flood hazard assessment in eastern Makkah city, Saudi Arabia. *Journal of King Saud University - Science*, *34*(4), 102045. https://doi.org/10.1016/j.jksus.2022.102045

EMO: A high-resolution multi-variable gridded meteorological data set for Europe. European Commission. (n.d.). European Commission. https://data.jrc.ec.europa.eu/dataset/0bd84be4-cec8-4180-97a6-8b3adaac4d26

Fekete, A., & Sandholz, S. (2021). Here Comes the Flood, but Not Failure? Lessons to Learn after the Heavy Rain and Pluvial Floods in Germany 2021. *Water*, *13*(21), Article 21. https://doi.org/10.3390/w13213016

Feyen, L., Vrugt, J. A., Nualláin, B. Ó., van der Knijff, J., & De Roo, A. (2007). Parameter optimisation and uncertainty assessment for large-scale streamflow simulation with the LISFLOOD model. *Journal of Hydrology*, *332*(3), 276–289. https://doi.org/10.1016/j.jhydrol.2006.07.004

Fifth Assessment Report—Synthesis Report. (n.d.). Retrieved January 31, 2023, from https://archive.ipcc.ch/report/ar5/syr/

Gai, L., Nunes, J. P., Baartman, J. E. M., Zhang, H., Wang, F., de Roo, A., Ritsema, C. J., & Geissen, V. (2019). Assessing the impact of human interventions on floods and low flows in the Wei River Basin in China using the LISFLOOD model. *Science of The Total Environment*, *653*, 1077–1094. https://doi.org/10.1016/j.scitotenv.2018.10.379

Global Lakes and Wetlands Database: Large Lake Polygons (Level 1). (2004, July 1). https://www.worldwildlife.org/publications/global-lakes-and-wetlands-database-large-lake-polygons-level-1

Harvard Dataverse. (n.d.). *Global Spatially-Disaggregated Crop Production Statistics Data for 2010 Version 2.0.* Harvard Dataverse. https://dataverse.harvard.edu/dataset.xhtml?persistentId=doi:10.7910/DVN/PRFF8V

Hdeib, R., Moussa, R., Colin, F., & Abdallah, C. (2021). A new cost-performance grid to compare different flood modelling approaches. *Hydrological Sciences Journal*, *66*(3), 434–449. https://doi.org/10.1080/02626667.2021.1873346

Hirpa, F. A., Salamon, P., Beck, H. E., Lorini, V., Alfieri, L., Zsoter, E., & Dadson, S. J. (2018). Calibration of the Global Flood Awareness System (GloFAS) using daily streamflow data. *Journal of Hydrology*, *566*, 595–606. https://doi.org/10.1016/j.jhydrol.2018.09.052

Huizinga, H. J. (2007). *Flood damage functions for EU member states. Technical Report, HKV Consultants.* HKV Consultants and Joint Research Center.

ISRIC World Soil Information. (n.d.). https://www.isric.org/about

Knighton, J., Buchanan, B., Guzman, C., Elliott, R., White, E., & Rahm, B. (2020). Predicting flood insurance claims with hydrologic and socioeconomic demographics via machine learning: Exploring the roles of topography, minority populations, and political dissimilarity. *Journal of Environmental Management*, *272*, 111051. https://doi.org/10.1016/j.jenvman.2020.111051

LISFLOOD Model Documentation. (n.d.). https://ec-jrc.github.io/lisflood-model/

LISFLOOD User Guide. (n.d.). https://ec-jrc.github.io/lisflood-model/

Mohr, S., Ehret, U., Kunz, M., Ludwig, P., Caldas-Alvarez, A., Daniell, J. E., Ehmele, F., Feldmann, H., Franca, M. J., Gattke, C., Hundhausen, M., Knippertz, P., Küpfer, K., Mühr, B., Pinto, J. G., Quinting, J., Schäfer, A. M., Scheibel, M., Seidel, F., & Wisotzky, C. (2022). A multi-disciplinary analysis of the exceptional flood event of July 2021 in central Europe. Part 1: Event description and analysis. *Natural Hazards and Earth System Sciences Discussions*, 1–44. https://doi.org/10.5194/nhess-2022-137

Peredo, D., Ramos, M.-H., Andréassian, V., & Oudin, L. (2022). Investigating hydrological model versatility to simulate extreme flood events. *Hydrological Sciences Journal*, *67*(4), 628–645. https://doi.org/10.1080/02626667.2022.2030864

Quirogaa, V. M., Kurea, S., Udoa, K., & Manoa, A. (2016). Application of 2D numerical simulation for the analysis of the February 2014 Bolivian Amazonia flood: Application of the new HEC-RAS version 5. *Ribagua*, *3*(1), 25–33. https://doi.org/10.1016/j.riba.2015.12.001

Reuters. (2022, July 18). Climate change extreme weather costs Germany billions annually. *Reuters*. https://www.reuters.com/world/europe/climate-change-extreme-weather-costs-germany-billions-euros-year-study-2022-07-18/

Ruijsch, J., Verstegen, J. A., Sutanudjaja, E. H., & Karssenberg, D. (2021). Systemic change in the Rhine-Meuse basin: Quantifying and explaining parameters trends in the PCR-GLOBWB global hydrological model. *Advances in Water Resources*, *155*, 104013. https://doi.org/10.1016/j.advwatres.2021.104013

Kling-Gupta Efficiency. (2019). Agricultural and Meteorological Software. https://agrimetsoft.com/calculators/Kling-Gupta%20efficiency#

Ryan, P., Syme, B., Gao, D. S., & Collecutt, D. G. (2022). Direct Rainfall Hydraulic Model Validation. *2022*.

Seifert, I., Botzen, W. J. W., Kreibich, H., & Aerts, J. C. J. H. (2013). Influence of flood risk characteristics on flood insurance demand: A comparison between Germany and the Netherlands. *Natural Hazards and Earth System Sciences*, *13*(7), 1691–1705. https://doi.org/10.5194/nhess-13-1691-2013

Shustikova, I., Domeneghetti, A., Neal, J. C., Bates, P., & Castellarin, A. (2019). Comparing 2D capabilities of HEC-RAS and LISFLOOD-FP on complex topography. *Hydrological Sciences Journal*, *64*(14), 1769–1782. https://doi.org/10.1080/02626667.2019.1671982

Sixth Assessment Report—IPCC. (n.d.). Retrieved January 31, 2023, from https://www.ipcc.ch/assessment-report/ar6/

Surminski, S., & Thieken, A. H. (2017). Promoting flood risk reduction: The role of insurance in Germany and England. *Earth's Future*, *5*(10), 979–1001. https://doi.org/10.1002/2017EF000587

Tom, R. O., George, K. O., Joanes, A. O., & Haron, A. (2022). Review of flood modelling and models in developing cities and informal settlements: A case of Nairobi city. *Journal of Hydrology: Regional Studies*, *43*, 101188. https://doi.org/10.1016/j.ejrh.2022.101188

Van Der Knijff, J. M., Younis, J., & De Roo, A. P. J. (2010). LISFLOOD: A GIS-based distributed model for river basin scale water balance and flood simulation. *International Journal of Geographical Information Science*, *24*(2), 189–212. https://doi.org/10.1080/13658810802549154

Wang, Y., Zhang, X., Tang, Q., Mu, M., Zhang, C., Lv, A., & Jia, S. (2019). Assessing flood risk in Baiyangdian Lake area in a changing climate using an integrated hydrological-hydrodynamic modelling. *Hydrological Sciences Journal*, *64*(16), 2006–2014. https://doi.org/10.1080/02626667.2019.1657577